Wintertime Precipitation Episodes in Central Chile: Associated Meteorological Conditions and Orographic Influences

MARK FALVEY AND RENÉ GARREAUD

Departamento de Geofísica, Universidad de Chile, Santiago, Chile

(Manuscript received 14 February 2006, in final form 2 June 2006)

ABSTRACT

Central Chile (32°–35°S) is a mountainous and densely populated strip of land between the South American Pacific coast and the main divide of the Andes, 5000 m in height. In this study, wintertime precipitation episodes in central Chile are characterized using precipitation gauge, river discharge, radiosonde, and Special Sensor Microwave Imager (SSM/I) passive microwave radiometer observations over a 10-yr period (1993–2002). Precipitation episodes that typically occur as cold frontal rainstorms move over the region from west to east, within which the cross-mountain flow is blocked at lower levels. The influence of the Andes on the climatological precipitation pattern extends several hundred kilometers upstream of the coast. Over the mainland, the wintertime precipitation is most strongly related to the height of the mean topography surrounding the rain gauge sites, rather than the actual altitudes of the instruments, although higher-elevation locations are not well sampled by available rainfall observations. Between the coast and foothills of the Andes, the precipitation pattern is relatively uniform despite the complex coastal topography. On the western face of the Andes climatological enhancement factors of between 1 and 3 are inferred.

Regression analysis against radiosonde data at a coastal site reveals that the precipitation is strongly related to the zonal (cross mountain) moisture flux. The strongest relationship is found when the moisture flux is multiplied by the relative humidity. This variable explains 50% of the variance in daily area average precipitation in central Chile and up to 60% of the variance in the daily precipitation recorded at individual stations. The factors contributing to events of heavy precipitation enhancement in the Andes were examined. Events of heavy, but isolated, precipitation in the Andes tend to occur in the warmer, prefrontal sector of approaching storms and are associated with unusually high moisture fluxes near to and above the crest of the mountain range. Strongly frontal episodes, characterized by widespread rainfall throughout central Chile, lead to variable, but on average rather weak, enhancement in the Andes.

1. Introduction

Over half of Chile's population of 15 million live within a small central zone (Fig. 1) between the latitude limits 32° and 35°S, bounded to the west by the Pacific coast and to the east by the main divide of the Andes mountain range (5000 m). This part of Chile is semiarid and its inhabitants are very much dependent on the 350 mm or so of annual rainfall (Rutllant and Fuenzalida 1991) that falls predominantly during the winter months of April to September. Wintertime rainfall episodes are also a frequent cause of disruption in the capital city of Santiago (population 6 million) and in other urban centers. The most intense episodes have led to flooding, landslides, and loss of life (Garreaud and Rutllant 1996). Meltwater from the Andean snowpack is the region's principal source of drinking water and irrigation during the dry season (Corripio and Purves 2005).

The strong seasonality of precipitation in central Chile results from the wintertime retreat of the South Pacific anticyclone that prevails over the region during summer (Saavedra and Foppiano 1992), exposing the region to sporadic frontal rainstorms embedded within baroclinic disturbances crossing the continent to the south. There are several major storms each winter that have a large variability in both the intensity and spatial distribution of the precipitation produced. Rutllant and Fuenzalida (1991) found that the presence of blocking anticyclones in the Bellingshausen Sea (60°S, 90°W) favors precipitation in central Chile by driving midlatitude cyclones well northward of their usual trajectories. Over interannual time scales, annual precipitation in

Corresponding author address: Dr. Mark Falvey, Departamento de Geofísica, Universidad de Chile, Blanco Encalada 2002, Santiago, Chile.
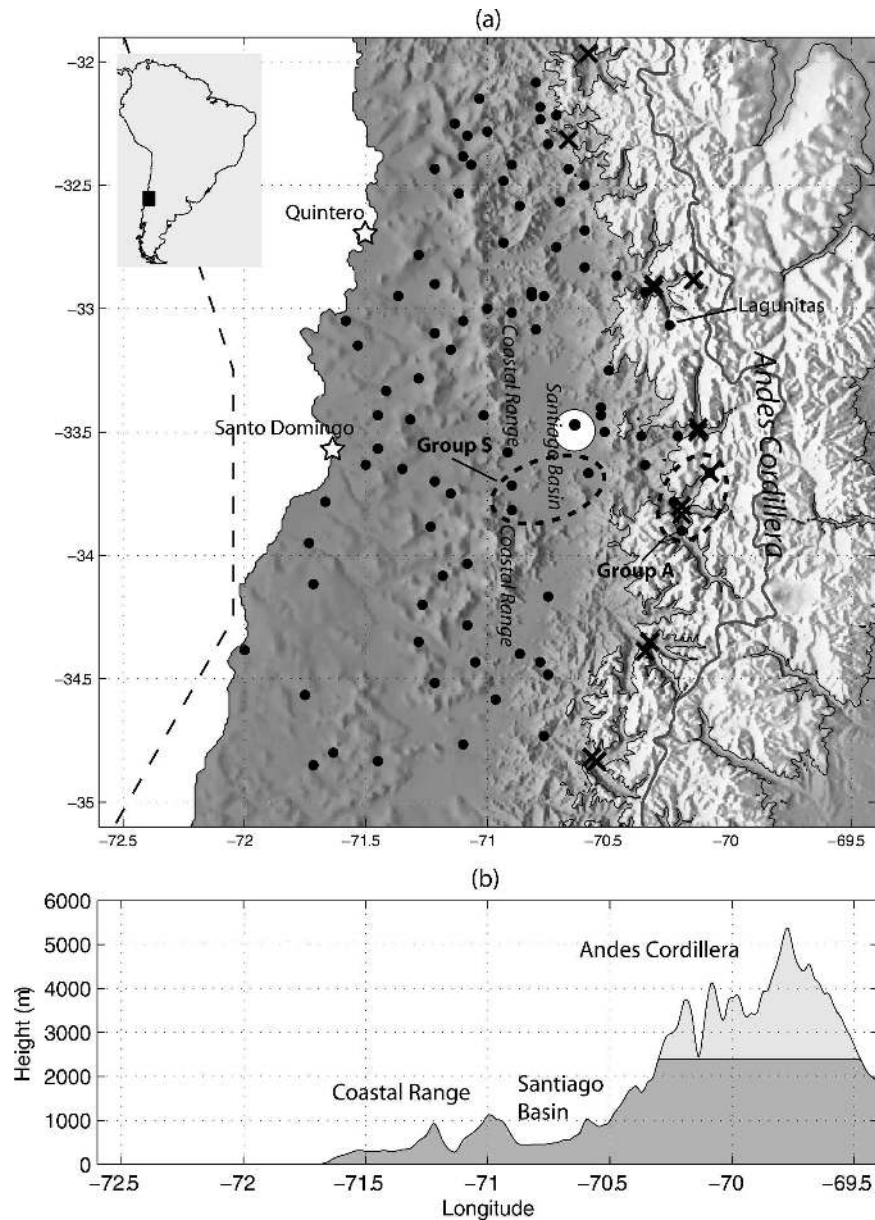E-mail: falvey@dgf.uchile.cl

FIG. 1. (a) The topography of central Chile and geographical locations referred to in the text. Black dots mark the locations of precipitation gauges. Crosses indicate the Andean river gauges. The stars show the locations of the Qunitero and Santo Domingo radiosonde sites. The large white circle indicates the approximate location and size of the city of Santiago. The black line that marks the boundary between darker and lighter topographic shading is the 2500-m elevation contour, which is at the approximate mean height of the wintertime snow line. The border with Argentina (gray line) roughly follows the main divide of the Andes. The dashed line west of the Chilean coast indicates the reference ($d = 0$) used to calculate the horizontal axes of the plots in Fig. 4. Groups A and S refer to the rain gauge station groups used in section 6. The map inset in the top left shows the location of central Chile (black rectangle) in South America. (b) The mean topography along a 10-km-wide section at 33.35°S.

central Chile shows a striking range (between 100 and 700 mm in Santiago), with wet (dry) years having a well-documented association with the El Niño (La Niña) phases of the Southern Oscillation (e.g., Acei-

tuno 1988; Montecinos et al. 2000; Montecinos and Aceituno 2003; Grimm et al. 2000; amongst others).

While the synoptic-scale and climatological forcing of precipitation in central Chile have been reasonably well

studied, comparatively little has been documented on the local forcing. Given the complex, high-altitude topography of the region, which includes not only the impressive Andes Cordillera (mountain range), but also a coastal mountain range and central basin, orographic precipitation processes may exert strong control over local rainfall patterns (e.g., Smith 1979; Banta 1990; Houze 1993). In the city of Mendoza, Argentina (33°S, 69°W), situated at a similar latitude and altitude to Santiago on the eastern side of the Andes, the wintertime precipitation amounts to only about 70 mm, less than a quarter of that in Santiago. Thus, in the broadest sense, the Andes of central Chile exhibit a rainfall pattern typical of midlatitude mountain ranges: a rainier zone on the upwind side and drier region in the lee (Roe 2005). Nonetheless, the shape of the rainfall distribution across the Andes, the extent of their upstream influence, and the existence of rainfall enhancement or shadow zones related to the coastal topography is not well known. This is in part due to the difficulty of obtaining long-term precipitation records in the inaccessible terrain, particularly at higher altitudes where the surface is snow covered during winter.

The intention of this article is to examine the characteristics of precipitation in central Chile and its associated meteorological forcing with an emphasis on the identification of orographic influences. Our study relies primarily on daily datasets for the 10 winters between 1993 and 2002, which include observations from a coastal radiosonde, a network of 88 precipitation gauges, and passive microwave radiometer. We dedicate a section of this study to the analysis of episodes of unusually enhanced or suppressed precipitation in the Andes Cordillera.

The structure of this article is as follows. In the next section the observational data are described. In section 3 the rainfall-related datasets are used to characterize the long-term spatial distribution of rainfall over central Chile. In section 4 we examine the meteorological characteristics of rainfall events in the region. The statistical relationships between and upstream airmass properties are then examined in section 5. In section 6 we examine in more detail the factors governing precipitation enhancement in the Andes Cordillera. Some aspects of the results are discussed in section 7, and conclusions are presented in section 8.

2. Study area and data

a. Geographical setting

The region of interest is the part of continental Chile bounded to the north and south by the latitude limits of 32° and 35°S and to the east and west by the Pacific coast and the international border with Argentina (Fig. 1a). The most prominent geographical feature of the region is the Andes Cordillera whose main ridge runs north to south about 170 km east of the coast. The Andes form a roughly two-dimensional barrier, with an approximate barrier height (h_m) of 5000 m and a half-width (l_m) of 50 km, implying an orography that is hydrodynamically steep under stable atmospheric conditions (Overland and Bond 1995). The Andes are mostly snow covered during the winter months, with the snow line typically found at 2500-m altitude.

Other notable topographic features include the coastal range ($h_m \sim 1200$ m, $l_m \sim 30$ km), with individual peaks exceeding 2000 m in height, oriented roughly parallel to the Andes about 60 km inland from the coast and the Santiago basin that sits between the coastal range and the Andes. Both these features are most clearly delineated in the central part of the study area. We emphasize that although the topography of the coastal range is dwarfed by the Andes Cordillera, orographic enhancement has been observed in many mountain ranges of equivalent (or smaller) dimensions, a relevant example being the coastal range of California (Neiman et al. 2002).

b. Observational data

The time period for this study includes the 10 winters (April–September) from 1993 to 2002. Unless otherwise stated, all observational data described in the subsections below span this period.

1) RAIN GAUGE

Daily rainfall data were available at 88 sites (Fig. 1). Most rain gauges are simple, nonautomated instruments, read manually by local observers at 1200 UTC (0800 local time). All data series were more than 95% complete, and any missing observations were replaced by those at the nearest station. The spatial sampling is nonuniform, with gaps in the Santiago basin, the northwestern coast, and the highest elevation parts of the coastal range. In the Andes Cordillera the few available sites are generally found within deep canyons at altitudes that are well below that of the mean surrounding topography. Daily records of snowfall in the Andes were available at a single site (Lagunitas, 2765 m), where manual measurements of depth and density are made at 3-h intervals and later summed into daily totals.

2) RIVER GAUGE

River discharge data provide an alternative means of estimating the mean precipitation in high-altitude wa-

TABLE 1. The columns latitude, longitude, and height refer to the location of the river discharge measurements; H_{mean} is the mean topographic height within the watershed; A is the watershed area; A_{snow} is the surface area of the watershed above the mean altitude of the winter snow line (2400 m); Q is the annual mean discharge; and R_{W1}^* and R_{W2}^* are the upper and lower limits for the mean wintertime precipitation calculated using the methods described in the appendix.

Watershed	Latitude	Longitude	Height (m)	H_{mean} (m)	A (km^2)	A_{snow} (km^2)	Q (m^3 s^{-1})	R_{W1}^* (mm)	R_{W2}^* (mm)
Alicahuae	32.32°S	70.67°W	1780	3330	224	141	0.75	95	288
Choapa	31.97°S	70.58°W	1200	2610	1091	983	8.35	217	490
Juncal	32.88°S	70.15°W	1800	3930	233	232	5.83	710	989
Blanco	32.92°S	70.32°W	1420	3710	380	360	9.68	723	986
Aconcagua	32.90°S	70.32°W	1420	3630	875	835	20.4	661	929
Colorado	33.50°S	70.13°W	1500	3890	834	511	16.2	551	827
Olivares	33.48°S	70.13°W	1500	3880	531	397	8.1	433	714
Miapo	33.83°S	70.20°W	1527	3330	1488	1343	40.7	776	1022
Volcan	33.80°S	70.20°W	1365	3560	523	483	15.7	852	1101
Yeso	33.67°S	70.08°W	2475	3970	353	353	8.1	651	934
Cachapoel	34.38°S	70.35°W	1188	3140	476	403	23.5	1401	1594
Cortaderal	34.35°S	70.33°W	1200	3110	382	323	21.0	1560	1749
Tinguiririca	34.83°S	70.55°W	1032	2870	370	275	16.7	1281	1452
(Azufre)	34.82°S	70.57°W	1024	3060	978	786	35.1	1019	1221
Tinguiririca	32.32°S	70.67°W	1780	3330	224	141	0.75	95	288

tersheds of the Andes where rain gauge observations are sparse. The basic premise is that, over time scales of several years or more, the net change in basin water storage is zero, and the mean precipitation in the basin is approximately balanced by the mean river discharge at the outlet point of the basin. That is,

$$R^* \sim Q/A, \qquad (1)$$

where R^* is the mean annual catchment rainfall, Q is the mean annual discharge, and A is the area of the catchment. Of course, this highly simplified conceptualization neglects the fact that substantial water may be removed from the catchment by evaporation and infiltration. However, the methodology does provide a plausible means of obtaining a lower limit for bulk precipitation in the catchment.

We consider data from 12 high-altitude Andean watersheds where reliable mean annual (January–December) discharge measurements were available for a 30-yr period from 1961 to 1990 (Fig. 1 and Table 1). Precipitation data presented in Carrasco et al. (2005) show that at low-lying stations in central Chile the mean annual precipitation during this time was similar (within 10%) to that during our study period of 1993–2002. Long-term records were also available on an elevated site in the Maipo Valley (1195 m), and the mean annual precipitation there was also found to be very similar for the 1961–90 (719 mm) and 1993–2002 (688 mm) periods. While these rain gauge observations are not necessarily representative of the high-altitude watersheds in the Andes, they do give some credibility to the notion that rainfall estimates derived from the river discharge data

may be usefully compared with other precipitation data in this study.

The annual river discharges were used to make "ball-park" estimates of lower and upper limits (R_{w1}^* and R_{w2}^*, respectively) for mean winter rainfall in each catchment, using a simple methodology described in detail in the appendix. The lower limit (R_{w1}^*) is based on essentially the same formulation as that described above, with a minor correction to account for the ratio of summer to winter rainfall. The upper limit (R_{w2}^*) includes a rough estimate of water loss due to evaporation.

3) SSM/I PASSIVE MICROWAVE RADIOMETER

The Special Sensor Microwave Imager (SSM/I) passive microwave radiometer onboard the Defense Meteorological Satellite Program (DMSP) satellites has provided an abundant source of meteorological information over the World's Oceans since the launch of the first instrument in 1987. We make use of SSM/I oceanic datasets of precipitation and precipitable water (PW) provided by Remote Sensing Systems (RSS; http://www.ssmi.com). RSS use a physical inversion algorithm that simultaneously retrieves the total precipitable water content, total cloud water, sea surface temperature, surface wind magnitude, and rainfall rate (Wentz 1997). During the study period five SSM/I radiometers were operational over various intervals, aboard the DMSP *F10* (1993–97), *F11* (1993–2000), *F13* (1995–2002), *F14* (1997–2002), and *F15* (1999–2002) satellites. At RSS, estimates of each atmospheric variable from ascending and descending orbits for each satellite are mapped onto a global 0.25° × 0.25° grid. We further combined

these data to form daily mean fields (1200 UTC until 1200 UTC the day after), averaged over the ascending and descending observations from all instruments, at the same spatial resolution. Typically each daily grid-point estimate is an average of about four instantaneous SSM/I observations. Further information on remote sensing with SSM/I may be found in Smith et al. (1998).

The SSM/I precipitation estimates are not calibrated against local data, and scarcity of rainfall over the southeast Pacific prohibits any meaningful validation. The climatological rainfall parameters derived from the SSM/I data used in the next section may suffer from biases due to errors in the retrieval algorithm, screening of light rainfall, and undersampling (Berg and Avery 1995; Bell and Kundu 2000). For this reason, we avoid any direct comparison of the satellite precipitation estimates with gauge-measured rainfall, and SSM/I precipitation data are principally used for the detection of rainy areas.

4) RADIOSONDE

Radiosonde observations of winds, pressure, temperature, and humidity are made twice daily (0000 and 1200 UTC) at the coast of central Chile. Until 23 September 1998 the instrument was located at Quintero (Fig. 1), after which it was shifted some 80 km south to Santo Domingo. Inspection of the radiosonde data reveals that the shift in station location has minimal effect on the values of most meteorological variables during precipitation events. In particular, the statistical results to be discussed in section 5 were found to be effectively the same when using only radiosonde observations at either Quintero or Santo Domingo. Therefore, in the remainder of this article we will make no attempt to distinguish observations from the two sites and both will be referred to in the same way as the "coastal radiosonde."

Observations were obtained from synoptic reports on standard and significant levels, archived and disseminated by the University of Wyoming (http://weather.uwyo.edub). All meteorological variables were interpolated linearly to a vertical grid spaced at 100-m intervals between 100 and 8000 m above the surface. The main use of the radiosonde data is in the analysis of 24-h rainfall accumulations recorded at 1200 UTC. To obtain corresponding daily mean profiles from the original 12 hourly observations each variable (V) at a given level i was averaged according to

$$V_0 = (V_{-12h} + 2V_0 + V_{+12h})/4 \qquad (2)$$

where V_{-12h} and V_{+12h} are observations 12 h before and 12 h after the radiosonde observation at 0000 UTC (V_0); V_0 is given twice the weighting of the other observations reflecting its position in the center of the averaging period. All radiosonde data presented in this article are from daily profiles generated using this averaging scheme.

3. Long-term rainfall patterns

In this section we examine the long-term spatial pattern of precipitation in central Chile using the rain gauge, river gauge, and SSM/I datasets in terms of two summary measures of precipitation: the mean wintertime total (R_w) and the frequency of rainy days (R_f). Here R_W is defined simply as one-tenth of the total winter (April–September) precipitation recorded over the 10-winter (1993–2002) observation period. Typically, it accounts for between 85% and 95% of the annual total at most sites in central Chile. The measurement R_f is simply the percentage of winter days over the entire observation period in which nonzero precipitation was recorded. We caution that, since interannual rainfall variability is high in central Chile, neither R_W nor R_f can be expected to be representative of the rainfall distribution for any particular year.

Figure 2 shows the large-scale wintertime precipitation pattern over the southeastern Pacific based on SSM/I observations. The pattern is clearly dominated by the midlatitude storm track that passes over southern Chile during the winter months. Central Chile (black box in both Figs. 2a,b) is located well to the north of this feature, in a region of relatively infrequent synoptic activity and rapid northward decay in winter precipitation. Evident in both Figs. 2a,b is an elongated rainfall maximum within about 400 km of the coast (the western edge of this feature is identified subjectively with the dashed line) that stretches from central Chile (30°S) to the southern tip of the continent, implying a "far-field" impact of the continental orography. The enhancement of R_f in this zone suggests that rainy systems have a propensity to be triggered closer to the continent and/or that there is a deceleration (perhaps due to increased friction or topographic blocking) of existing rainy systems as they approach from the west. As the increase in R_W appears somewhat more abrupt than that of R_f, it may be that the intensity of rainfall also tends to increase toward the coast. It is noteworthy, although beyond the scope of this study to investigate further, that the zone maintains a relatively constant distance from the coast despite the large meridional variation in the effective barrier height of the Andes (Fig. 2c).
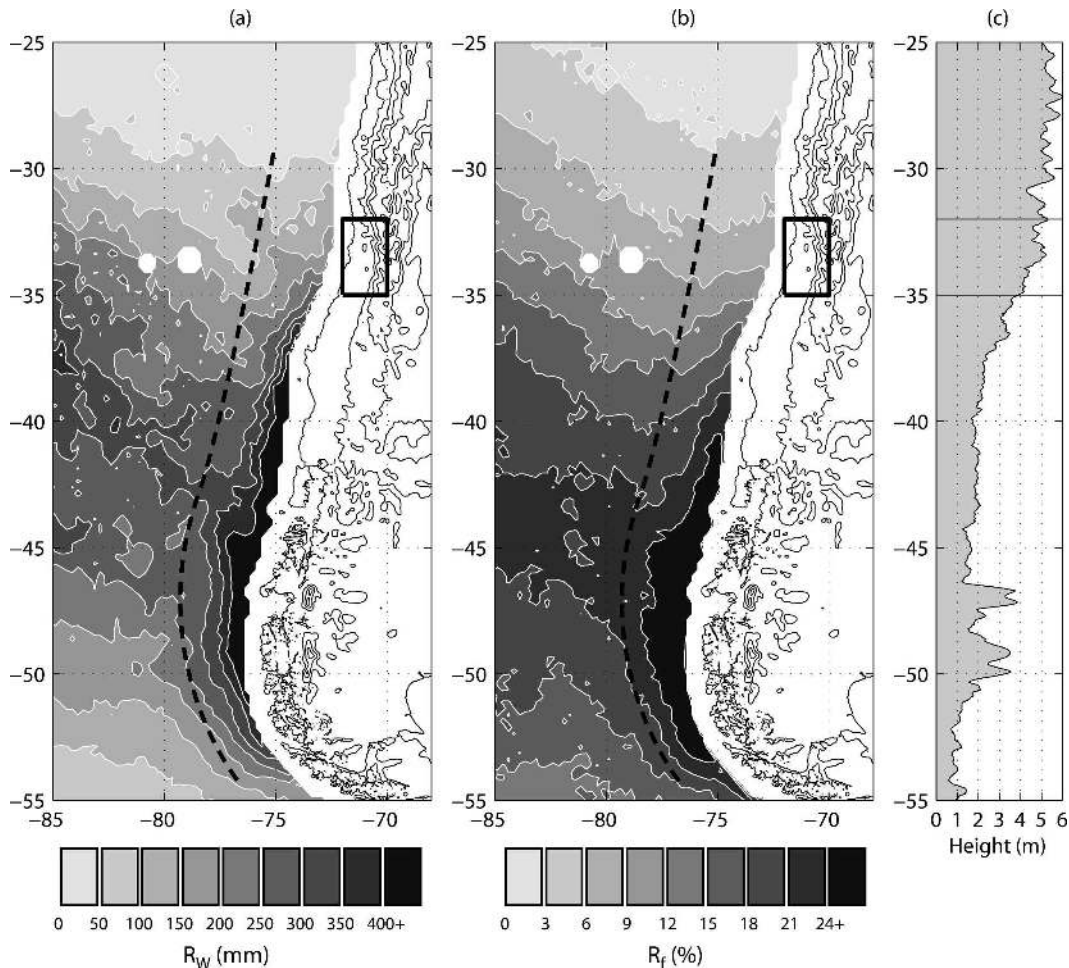
FIG. 2. (a) R_W and (b) R_f over the southeast Pacific Ocean derived from SSM/I rain-rate estimates. Here R_w is the mean wintertime precipitation between 1993 and 2002, and R_f is the percentage of days in which precipitation was recorded over this time period (again winter only). The box indicates the location of central Chile. The dashed line, determined subjectively, indicates the region where the continent appears to begin to influence the rainfall pattern. (c) The maximum height of the South American topography as a function of latitude smoothed to an effective resolution of 0.25°.

We focus now on the long-term characteristics of terrestrial rainfall in the study area. Figure 3 shows (a) the general spatial pattern of R_W and (b), (c) highlights meridional variation in R_W and R_f. The dominant spatial pattern in R_W is its marked northward decline, from about 500 mm at 35°S to 200 mm at 32°S (Fig. 3b). This is accompanied by a similar gradient in R_f (Fig. 3c), indicating that the winter rainfall pattern is largely determined by the synoptic-scale northward decay in the frequency of precipitation episodes. Along the Andes Cordillera the river gauge estimates of R_{W1}^* and R_{W2}^* show a similar, albeit sharper, northward decrease.

Figures 4a–c focus on the variation in the cross-mountain direction by plotting R_W and R_f along zonal cross sections through the northern, central, and southern parts of the study area. The definition of the three

cross sections is arbitrary and is intended to separate the central part of the study domain, where the coastal range and Santiago basin are readily discernible from the northern and southern parts where these topographic features are less evident. It is difficult to discern any clear relation between the winter rainfall pattern and the major orographic features in the Andes Cordillera. Between the coast and the foothills of the Andes, the distributions of both R_W and R_f are relatively uniform in each of three cross sections, despite the significant rises in terrain elevation along these transects. Examining the spatial distribution of precipitation (Fig. 3), there is possible evidence of an anomalously rainy zone in the hills south of the Quintero radiosonde station (Fig. 1). Otherwise, the rainfall distribution in the low-lying parts of central Chile shows
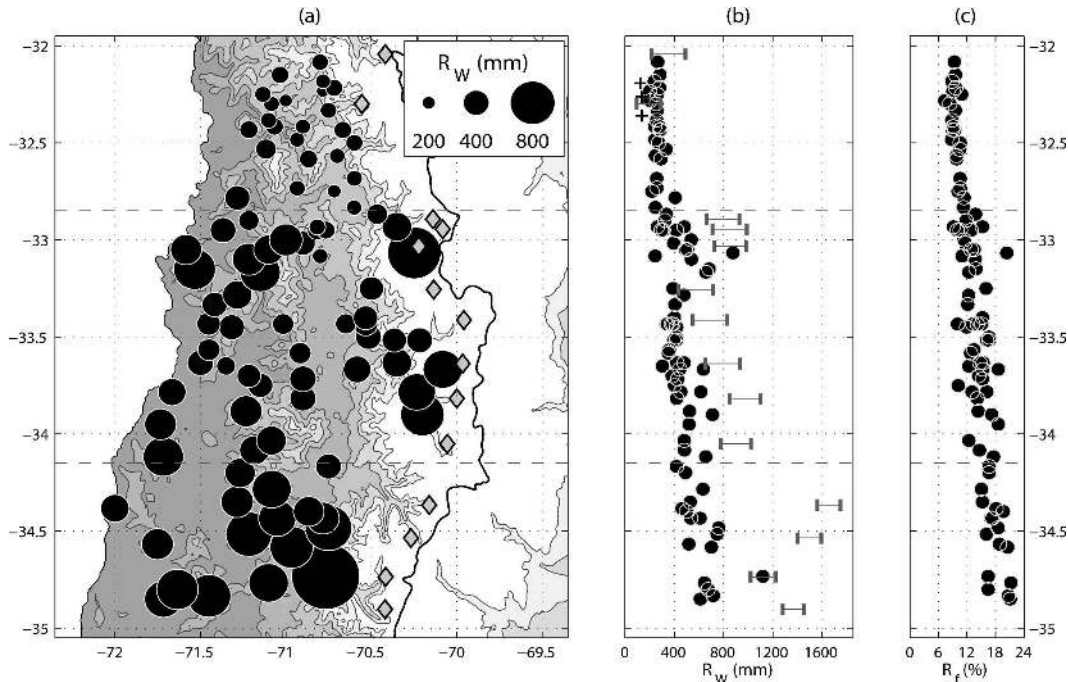
FIG. 3. (a) Black dots show rain gauge measurements of R_W, the radius of the circle being proportional to the R_W as indicated in the legend in the top right corner. Gray diamonds indicate the center points of the Andean watersheds (Table 1). (b) The variation of R_W with station latitude (black dots). Also shown are the lower and upper estimates of watershed precipitation R_{W1}^* and R_{W2}^* (left and right edges of the gray bars, respectively). The crosses indicate R_W from three stations in the Mendoza province of Argentina, whose longitudes (from north to south) are 68.8°, 68.5°, and 68.2°S. (c) The variation of R_f with station latitude. The dashed lines show the latitude limits for the northern, central, and southern cross sections plotted in Fig. 4.

little coherent spatial structure over and above the south–north gradient, although we acknowledge this conclusion is limited by the scarcity of rain gauge stations.

In the central cross section (Fig. 4b) instrumental coverage extends into the Andes, allowing the detection of a systematic increase in R_W associated with the sharp rise in topography. Eastward of the Santiago basin, the measured R_W increases to a maximum value of 900 mm at the Lagunitas snowfall site. The R_W does not show any clear relation to the station altitude (crosses in Fig. 4b) but appears to better follow the mean height of the cross section topography [Rasmussen and Tangborn (1976) noted a similar pattern in the north Cascades region of Washington]. The R_W data from the Andean precipitation gauges are reasonably consistent with the winter snowfall (R_W^*) estimates from the watersheds lining the western rim of the main divide, which range between 500 and 1500 mm. Viewed together, the rain and river gauge data suggest a climatological wintertime enhancement factor on the windward side of the Andes of 2 ± 0.5, with respect to the mean rainfall observed from the coast to the eastern edge of the Santiago basin. The frequency of precipita-

tion events is also greater in the Andes: the mean R_f being ~21% for stations where the mean topography is above 2500 m (i.e., distance along transect >120 km), compared to about 14% at sites between the base of the Andes to the coastal zone (shaded area at top of Fig. 4b), suggesting that at least some of the overall wintertime enhancement can be attributed to the occurrence of additional or prolonged rainfall episodes.

Due to the limited spatial sampling and high uncertainty of the precipitation estimates, the shape of the climatological rainfall profile across the central Andes cannot be determined. It is clear from the very small wintertime totals (~70 mm) in Argentina's province of Mendoza (Fig. 3b) that the trend of increasing precipitation on the upwind face of the Andes must reverse in the lee. However, it is unclear whether the climatological precipitation peak is found near to the main divide or somewhere on the upwind slopes as is generally the case for larger mountain ranges (Roe 2005). Moreover, the R_W^* estimates from the Andean watersheds show systematic variation in the direction perpendicular to the axis of the mountain range (Fig. 3b), which may undermine the applicability of the two-dimensional representation of the rainfall distribution.
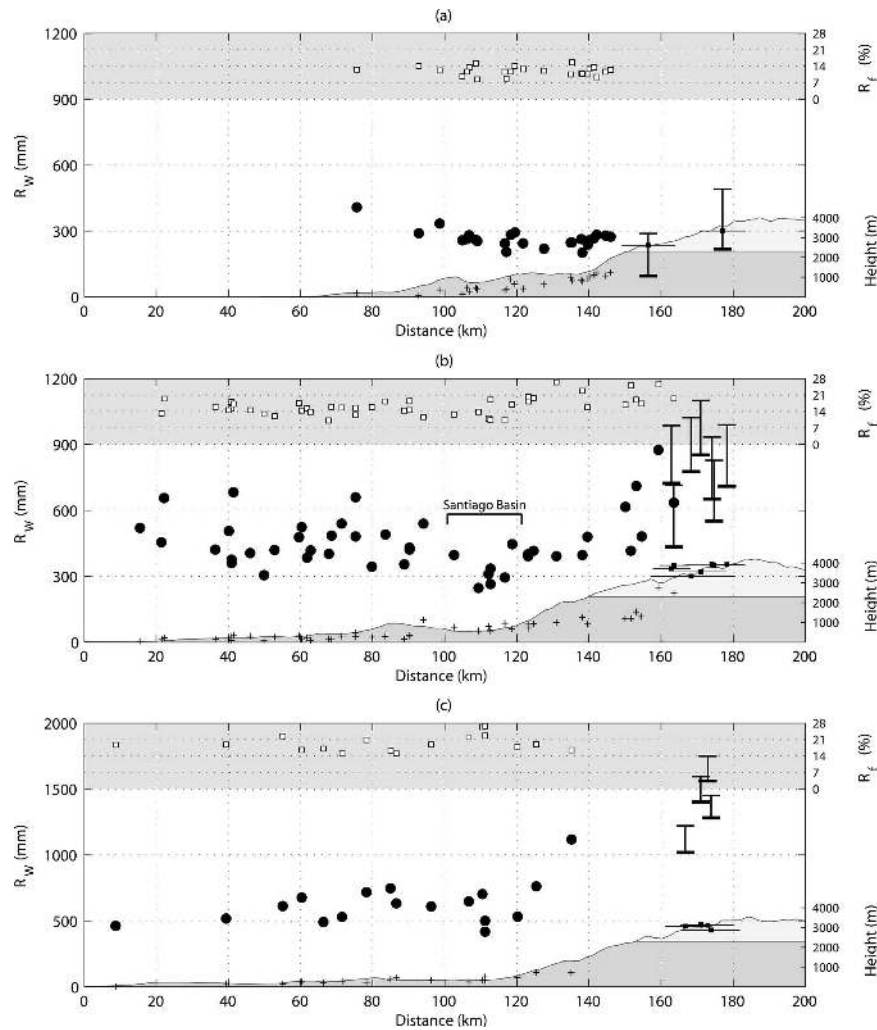
FIG. 4. Zonal cross sections of rainfall observations in the (a) northern (32°–32.85°S), (b) central (32.85°–34.15°S), and (c) southern (34.15°–35°S) parts of the study domain (see also Fig. 3). The horizontal axes are the distance from the reference line shown in Fig. 1, which roughly follows the shape of the main divide 180 km inland. Black dots show the values of R_W at each rain gauge. Vertical bars mark the lower and upper limits of the watershed rainfall estimates (R_{W1}^* and R_{W2}^*). The squares in the shaded section of (a)–(c) show R_f. The mean topography (gray region) is shown using the vertical scale on the bottom right of (a)–(c). Topography above the mean height of 2400 m [approx the height of the winter snow line in the central part (33.5°S) of the study area] is shaded light gray. The heights of precipitation gauges (crosses) and watershed center of mass (black dots with bar showing the along-transect extent of the watershed) are plotted on the same vertical scale.

The river gauge observations indicate that orographic enhancement increases to the south, where the precipitation estimated in the Andes exceeds that near the coast by a factor of almost 3 (Fig. 4c). To the north, precipitation enhancement appears to decrease dramatically (Fig. 4a). In the two northernmost watersheds the winter precipitation estimated, assuming a perfect balance with the river discharge (R_{W1}^*), is lower than that recorded by the rain gauges to the west. However, taking into account the considerable sublimation likely

to occur over winter, the actual R_W probably equals or exceeds that over the adjacent lowlands.

4. Meteorological conditions during rainfall episodes

In this section we examine the meteorological conditions associated with rainfall episodes in central Chile. Much of the following analysis will be based on a pool of 228 rainy days, hereafter referred to as "events,"

obtained by selecting all winter (April–September) days between 1993 and 2002 whose mean precipitation (P_m) averaged over all rain gauges was at least 1.0 mm and when at least 25% of rain gauges recorded nonzero precipitation. At each rain gauge site, the precipitation summed over the pool of events amounts to between 65% and 75% of the 10-winter total, and the mean spatial distribution is very similar to the overall winter distribution discussed in the previous section (not shown). The precipitation events frequently occur over consecutive days, so that the 228-element sample actually consists of 129 continuous episodes, of which nearly all (98%) lasted for 3 days or less.

a. Synoptic characteristics

We begin with some initial remarks regarding the synoptic characteristics shared by most events. This discussion is mainly based on subjective examination of synoptic maps [using National Centers for Environmental Prediction–National Center for Atmospheric Research (NCEP–NCAR) reanalysis (Kalnay et al. 1996)] and SSM/I fields of precipitable water, cloud water, and precipitation for each member of the event pool, augmented where possible by semiobjective methodologies such as cluster analysis (Wilks 1995), which we do not describe in detail for the sake of brevity.

Consistent with our expectations based on central Chile's climatological setting and the results of past studies, rainfall episodes are strongly associated with baroclinic disturbances south of the central zone. A midlevel trough south of central Chile (~40°S) and upper-level jet streak just to the north (~30°S) are synoptic features common to almost all episodes. Roughly 30% of precipitation events are associated with synoptic blocking scenarios of the sort described in Rutllant and Fuenzalida (1991). About 8% of events are connected with cutoff lows (COLs), closed midlevel (500 hPa) circulations having weak surface signatures (Fuenzalida et al. 2005) in agreement with Pizarro and Montecinos (2000), who concluded that between 5% and 10% of precipitation episodes in central Chile are associated with COLs. Other events are associated with cyclones (~26%) passing over southern Chile (between 40° and 60°S) or extended surface ridge–trough (~36%) systems.

A feature common to most (>85%) episodes is a cold frontal zone marking the boundary between the warm (northern) and cool (southern) sectors of the baroclinic wave. In the SSM/I imagery the fronts are manifest as marked discontinuities in the precipitable water field, typically oriented from NW to SE, that move west to east across central Chile during rainfall episodes. The fronts are associated with long cloud bands often, but not always, containing precipitation produced along the warm conveyor belt airstream, which ascends slantwise ahead of the surface front (Carlson 1998).

The mean time evolution of the frontal system is demonstrated in Figs. 5a–f, which show the composite anomaly sequence of SSM/I precipitation frequency and PW and the 700-hPa winds from reanalysis, starting 3 days before (t_{-3}) and ending 2 days after (t_{+2}) the day of precipitation occurrence (t_0). To test whether these "all event" composites are representative, we constructed similar sequences for several subsets of events (not shown), grouped according to their similarity in surface and 500-hPa geopotential fields. With the exception of a small group corresponding to the COL scenario, it was found that the subsetted anomaly patterns were very similar to the overall pattern shown in Fig. 5.

Three days prior to the central time (t_{-3}) (Fig. 5a), a cyclonic flow anomaly is positioned well to the west of central Chile (41°S, 87°W) with regions of positive PW and precipitation anomalies to the north. The long zonal extension of the latter features results from a high east–west variability in the locations of the associated fronts at this early stage in the sequence. Over the following days the anomaly pattern moves westward with constant velocity (~5 m s^{-1}) as the PW and precipitation anomalies strengthen (due to the increased consistency between events) and become inclined at 45° with respect to the zonal, reflecting the typical orientation of the approaching cold fronts. On the day prior to t_0 (Fig. 5c), the precipitation anomalies show a well-defined coastal maximum at 36°S, indicating that the fronts tend to make landfall just to the south of the study area. At this stage a northwesterly flow anomaly transports moist air of subtropical origin over central Chile, and there is a negative PW anomaly in the southwestern part of the cyclone resulting from the advection of cooler, drier air from higher latitudes. At time t_0 the circulation anomaly is centered slightly west of the coast at 37°S. Synoptic precipitation is concentrated in a small zone immediately to the west of central Chile, whose limited northward extent reflects the fact that precipitation usually occurs as the tip of the frontal rainband crosses the zone.

During the days following t_0 (Figs. 5e,f) the PW and precipitation anomalies disappear, indicative of a rapid weakening or dispersion of the frontal systems after their arrival in central Chile or that they have progressed eastward over the continent where SSM/I observations are not available. The cyclonic circulation anomaly weakens but remains centered on the western
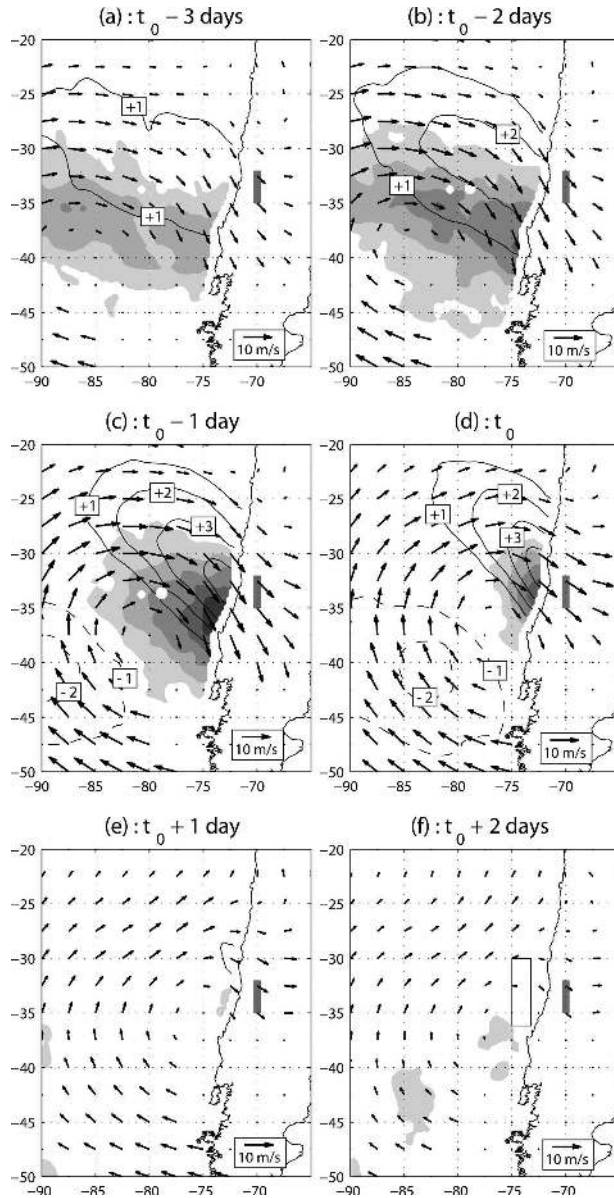
FIG. 5. (a)–(f) Sequence of composites beginning 3 days prior $(t_0 - 3)$ and ending 2 days after $(t_0 + 2)$ the sample of rainfall events. Arrows show the wind anomaly with respect to the winter mean at 700 hPa from NCEP–NCAR reanalysis. Solid (dashed) contours show positive (negative) precipitable water anomalies (mm) measured by SSM/I, again with respect to their winter mean values. Gray shading shows areas of positive SSM/I rainfall occurrence anomalies, defined as the percentage of events in which rain was recorded minus the mean percentage of rainy days during winter (R_f). The grayscale varies from 10% (lightest) to 30% (darkest). Negative anomalies are not shown. The gray bar indicates the location of central Chile. The box in (f) shows the region used to define the frontal precipitation index I_{front}.

TABLE 2. Index of frontal rainfall (I_{front}) and its relation to precipitation in central Chile, where I_{front} is defined as the percentage of SSM/I grid cells in which precipitation was observed within the boxed region shown in Fig. 5f. The rows of the table show some simple statistics related to the members of each quartile of I_{front}, which occupy the ranges of values shown in the second column. The columns labeled Mean (P) and Mean (F_{u2500}) show the mean precipitation averaged over all rain gauges and the mean value of zonal moisture flux at 2500 m, respectively.

I_{front}	Range (I_{front})	Mean (P) (mm)	Mean (F_{u2500}) (kg m^{-2} s^{-1})
1st quartile (lower)	0.0%–0.5%	6.3	3.5
2d quartile	0.5%–11.5%	10.2	4.2
3d quartile	11.5%–39.6%	16.0	7.0
4th quartile (upper)	39.6%–98.4%	20.0	8.1

side of the Andes, indicating that the westward advance of the baroclinic disturbance tends to be halted by the Andes.

We computed a simple frontal precipitation index (I_{front}) defined as the percentage of rainy SSM/I grid cells in the rectangular region well upstream of central Chile shown in Fig. 5f. Events with larger values of I_{front} are generally associated with more active systems producing widespread rainfall. The values of I_{front} were grouped into their four quartiles, and the average value of P_m (defined at the beginning of this section) was calculated for each. The result, shown in Table 2, demonstrates that as frontal precipitation increases upstream, so too does the precipitation in central Chile. The lowest quartile of I_{front}, which consists almost entirely of events in which no precipitation was observed upstream and therefore may be regarded as events of "pure" orographic precipitation, shows the lowest mean precipitation of 6.3 mm, well below the average over all events. The mean P_m increases to 20 mm for the upper I_{front} quartile, suggesting that the frontal component of precipitation may make a substantial, perhaps dominant, contribution to the daily totals observed in central Chile. Of course, interpretation is complicated by the intrinsic link between frontal precipitation and orographic enhancement, a point to be discussed further in section 7.

b. Local conditions

The mean atmospheric conditions at the coastal radiosonde during precipitation events are shown in Figs. 6a–f. We take these measurements as being representative of the conditions upstream of the coastal mountains and the Andes, although it must be recognized that conditions may vary systematically north to south along the 3° length of coastline that our study area contains. The prevailing winds are from the northwest
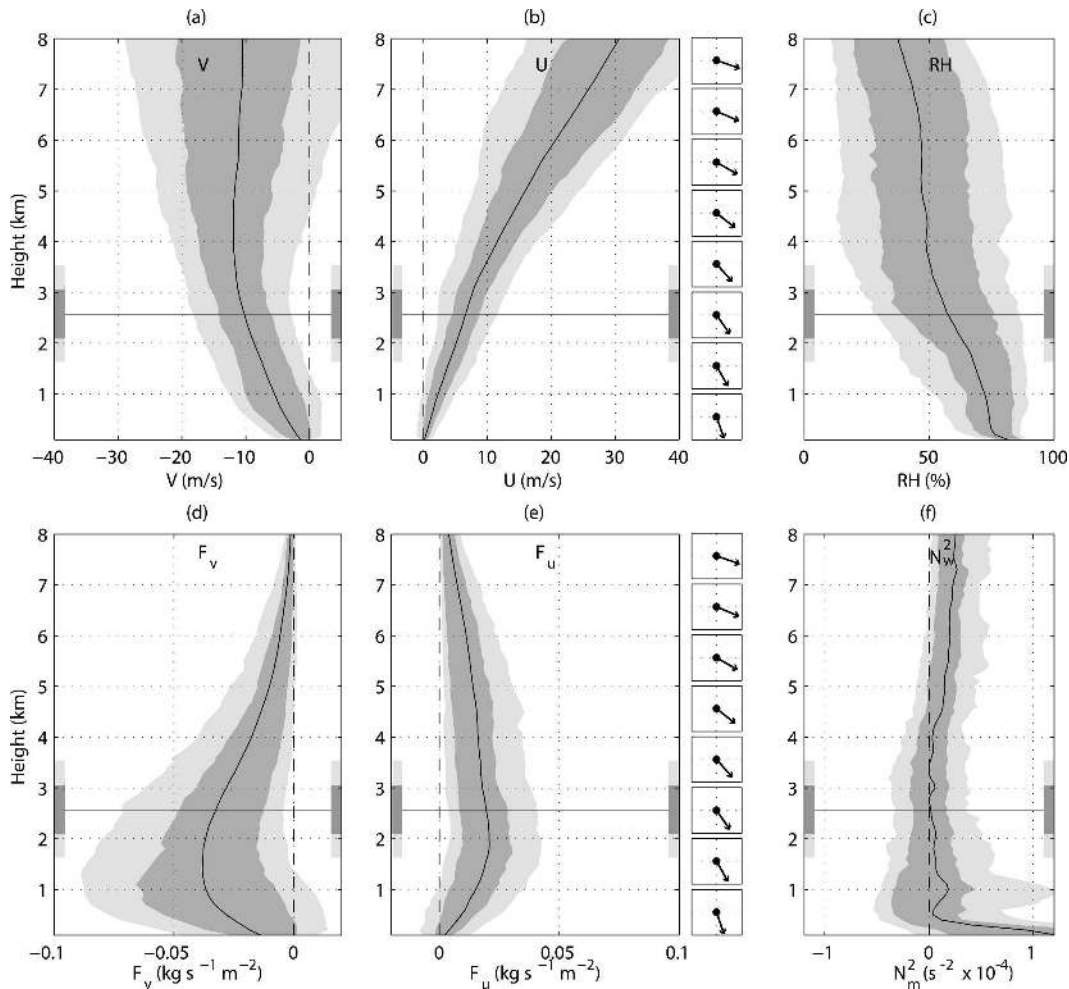
FIG. 6. (a)–(d) Vertical profiles of coastal radiosonde measurements of selected atmospheric variables during rainfall episodes. The solid line indicates the mean value, the dark gray region indicates the interquartile range, and the light gray region indicates the 5%–95% percentile range. The gray horizontal line is the mean height of the freezing level, and the dark and light gray bars on either side of the plot show its interquartile and 5%–95% percentile ranges, respectively. The arrows left of (a) and (d) indicate the direction of the wind and flux vectors. The variables are defined in Table 3.

(Figs. 6a,b), increasing in magnitude and backing with height from northerly close to the surface to near-westerly at the highest level shown (8000 m). A positive mean zonal (i.e., cross barrier) flow is seen throughout the profile (Fig. 6b), although it is relatively weak (<16 m s^{-1}) below the 5000-m ridge height of the Andes.

The vertical wind shear largely reflects the baroclinic nature of the precipitation episodes. However, because the radiosonde is located well within the Rossby radius (Overland and Bond 1995) of the Andes Cordillera, it seems likely that the northerly deceleration of flow at low levels may be at least partially attributed to blocking by the Andes. Blocking is expected to occur when the Froude number (F_r; see Table 3 for definition) of

the upstream air mass is less than unity (Smolarkiewicz and Rotunno 1990; Overland and Bond 1993). Noting that the zonal wind speed at the barrier height of the Andes ($h_m = 5000$ m) rarely exceeds 25 m s^{-1}, it is clear that the blocking criterion will be met when the ambient stability (N) exceeds the modest value of 5×10^{-3} s^{-1}. For unsaturated air masses this stability threshold is exceeded in all of the rainfall events; hence blocked conditions are more or less guaranteed in central Chile during precipitation episodes. Because water vapor is strongly concentrated in the lower atmosphere, the mean low-level northerly turning means that the moisture fluxes (**F**) are strongest in the mountain parallel direction (F_v) with a pronounced peak at 1500 m in altitude (Fig. 6d). The zonal (cross mountain) moisture

TABLE 3. Variables measured at coastal radiosonde site. Vector variables are given in bold type, and their zonal and meridional components are indicated by the symbols u and v, respectively; ρ_v is the water vapor density, g is the gravitational acceleration (9.81 m s^{-2}), θ is the potential temperature, and θ_0 is the potential temperature at the 1000-hPa reference level. The quantity h_m represents the height of an orographic barrier perpendicular to the wind velocity component u.

Variable	Symbol	Definition	Units
Wind velocity	**U**: (u, v)		m s^{-1}
Moisture flux	**F**: (F_u, F_v)	ρ_v**U**	kg m^{-2} s^{-1}
Moisture flux multiplied by relative humidity	**δF**: $(\delta F_u, \delta F_v)$	RH **F**	kg m^{-2} s^{-1}
Temperature	T		K
Specific humidity	q		0–1
Relative humidity	RH		%
Squared dry Brunt–Väisälä frequency	N^2	$(g/\theta_0)\, d\theta/dz$	s^{-2}
Squared moist Brunt–Väisälä frequency	N^2_m	Durran and Klemp [1982, their Eq. (36)]	s^{-2}
Froude no (dry)	F_r	$u/h_m N$	

flux (F_u) is much weaker and has a broader peak with a maximum value at 2100 m (Fig. 6e).

The mean profiles show low mean relative humidity, which varies from 75% at the surface dropping to only 50% above altitudes of 4000 m (Fig. 6c). The freezing level is generally between 1000 and 3000 m, with a mean altitude of 2000 m. The profile of mean N^2_m indicates a neutral or slightly positive stability for saturated air parcels between 500 and 4000 m (Fig. 6f). A more detailed examination shows that 85% of the N^2_m profiles for rainfall events have a layer of conditionally unstable air at least 500 m thick below 4000 m (not shown).

5. Empirical relationships between precipitation and upstream airmass properties

The precipitation intensity in zones of sloping orography has been shown to be strongly related to certain properties of the upstream air mass in several of the world's mountain ranges. In the basic "upslope flow" picture of orographic precipitation, where streamlines at all levels follow the shape of the underlying topography, the strength of the orographic updraft depends on the horizontal wind in the direction of the topographic gradient (Sinclair 1994; Pandey et al. 2000). Although this conceptual picture is highly simplified, the cross-barrier wind speed has been found to be a good indicator of orographic precipitation in mountain ranges in the midlatitudes [e.g., Hill et al. 1981 (Wales); Wratt et al. 2000 (New Zealand); Rasmussen et al. 2001 (Washington); Neiman et al. 2002 (coastal California)]. Since the amount of precipitation also depends on the available water supply, the cross-mountain flow has been expressed in terms of the moisture flux, sometimes weighted by the relative humidity (Pandey et al. 1999; Rasmussen et al. 2001; Hayes et al. 2002). Other airmass properties, such as the humidity, absolute water

vapor content, and stability, may also exhibit significant relationships to orographic precipitation (e.g., Wratt et al. 2000). In this section we examine the statistical relationships between daily rainfall intensity in central Chile and the upstream airmass properties obtained from the coastal radiosonde observations.

We consider the potential influences of 10 candidate variables, or *predictors*, including the scalar quantities: wind speed ($|U|$), moisture flux magnitude ($|F|$, $|\delta F|$), relative humidity (RH), specific humidity (q), temperature (T), and moist stability (N^2_m) along with the vector quantities: wind velocity (**U**), moisture flux (**F**), and humidity-weighted moisture flux (**δF**). The precise definitions and units of these variables are provided in Table 3. The predictors are evaluated at the radiosonde level closest to the surface (100 m) and at 500-m intervals between altitudes of 500 and 8000 m. Before analysis, each variable was first smoothed to an effective vertical resolution of 500 m using a moving average filter.

We begin by analyzing the mean daily precipitation (P_m) computed using all gauges. This serves as a simple measure of the area mean precipitation in central Chile, although it is weighted toward lower-lying regions where the instrumental sampling is best. Standard least squares methods were used to determine the linear relationship $P_m = aX + c$ (a and c being constants) between P_m and each predictor variable X. The strength of the linear relationship is measured by squared correlation coefficient (r^2). For the vector quantities, a two-parameter regression is used, that is, $P_m = aX_U + bX_V + c$. In this case, the constants a and b describe the component of the vector **X** that has the strongest relation to P_m.

To obtain reliable values of r^2, and an estimate of its significance, 500 realizations of r were evaluated for each predictor using the bootstrap technique (Efron
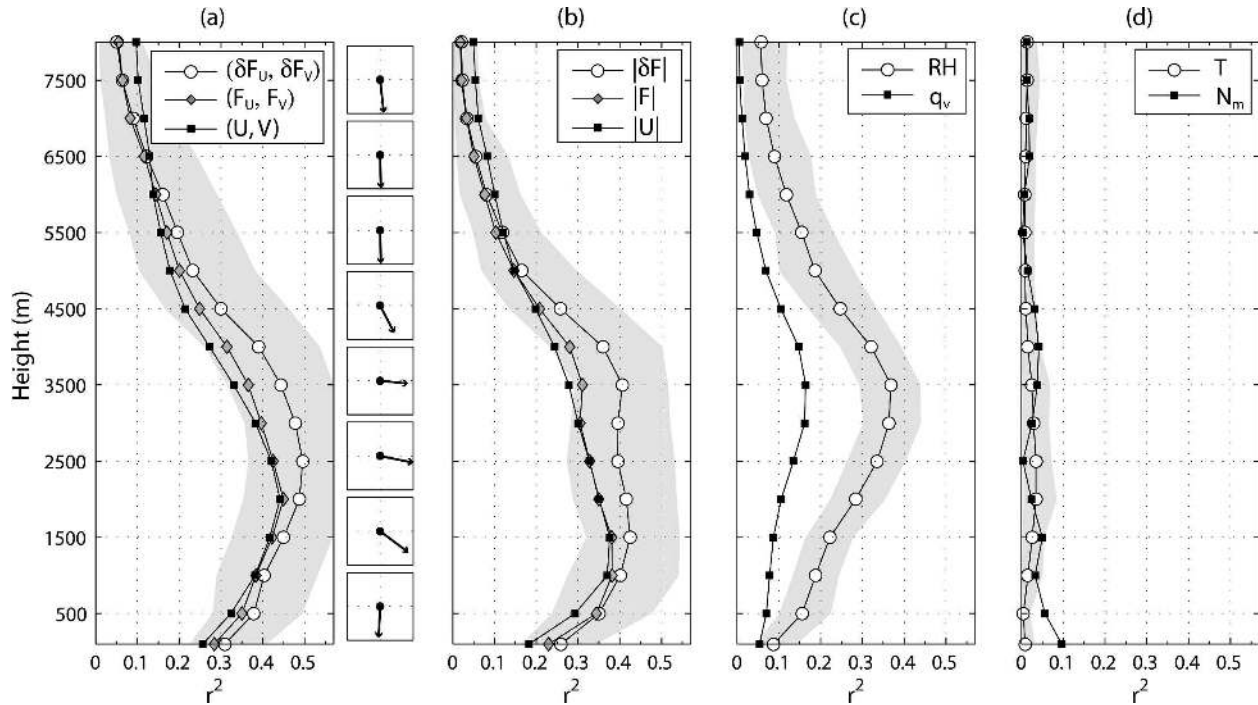
FIG. 7. Results of a linear fit between P_m and variables derived from the coastal radiosonde. The goodness of fit is measured by the r^2 statistic and is plotted as a function of height for each of the parameters tested. The gray region shows the 95% confidence region of r^2 for the predictors corresponding to the white circle symbols. The arrows to the right of (a) indicate the direction of the component of the flux vector (δF_U, δF_V) that gives the best fit to P_m.

and Tibshirani 1993), and the best estimate of r^2 was taken to be the mean value. Confidence intervals for r^2 are likewise determined from the pool of bootstrapped r estimates. Because the distribution of P_m is nonnormal (not shown), with a "tail" of unusually rainy events, there is some doubt regarding the robustness of statistical relationships derived using linear regression. We repeated the analysis several times after first transforming P_m by taking its square root (a methodology recommended by Wratt et al. 2000) and after removing the largest 3, 5, 10, and 20 events from the P_m vector. In all cases we obtained essentially the same results as those from the analysis with P_m unmodified, demonstrating that the empirical relationships shown below are robust and not overly influenced by abnormally intense events.

To visualize the results of the analysis we adopt a method similar to that used by Neiman et al. (2002), in which vertical profiles of r^2 are plotted as a function of height (Figs. 7a–d). Of all the predictors considered, the wind and moisture flux vectors (U, F, and δF) show the strongest correlations with P_m (Fig. 7a). Their vertical profiles of r^2 are characterized by a broad maximum in the lower troposphere between 100 and 5000 m, with the highest r^2 at 2000 m for U and F and at 2500 m for δF (Fig. 7a). The profiles of r^2 for U and F are quite

similar, suggesting that the positive correlation between rainfall and moisture flux is largely determined by the variability in the wind velocity. The δF variable gives consistently higher r^2 values at all levels, demonstrating that modulation of the moisture flux by the relative humidity leads to an improved relationship with precipitation. The regression parameters a and b, interpreted as vector components in the zonal and meridional directions, respectively, are similar for the all three flux predictors (arrows shown for δF in Fig. 7a). At lower ($\leq$1000 m) and higher ($>$4000 m) altitudes P_m correlates best with the northerly component of δF, while at intermediate levels, where r^2 is greatest, the orientation is conspicuously in the zonal (i.e., cross barrier) direction.

The magnitudes of the velocity and moisture flux predictors (U, F, and δF) also show significant correlations with P_m (Fig. 7b), although above 1000 m they are weaker than for their vector counterparts. The relative humidity (Fig. 7c) shows strongest relationships to P_m at altitudes well above the surface, with a maximum r^2 of 37% at 3500 m. The specific humidity (q_v), an absolute measure of water vapor content, correlates only weakly with P_m. Neither the temperature (T) nor the stability parameter N_m^2 show a significant linear relation to P_m at any level.
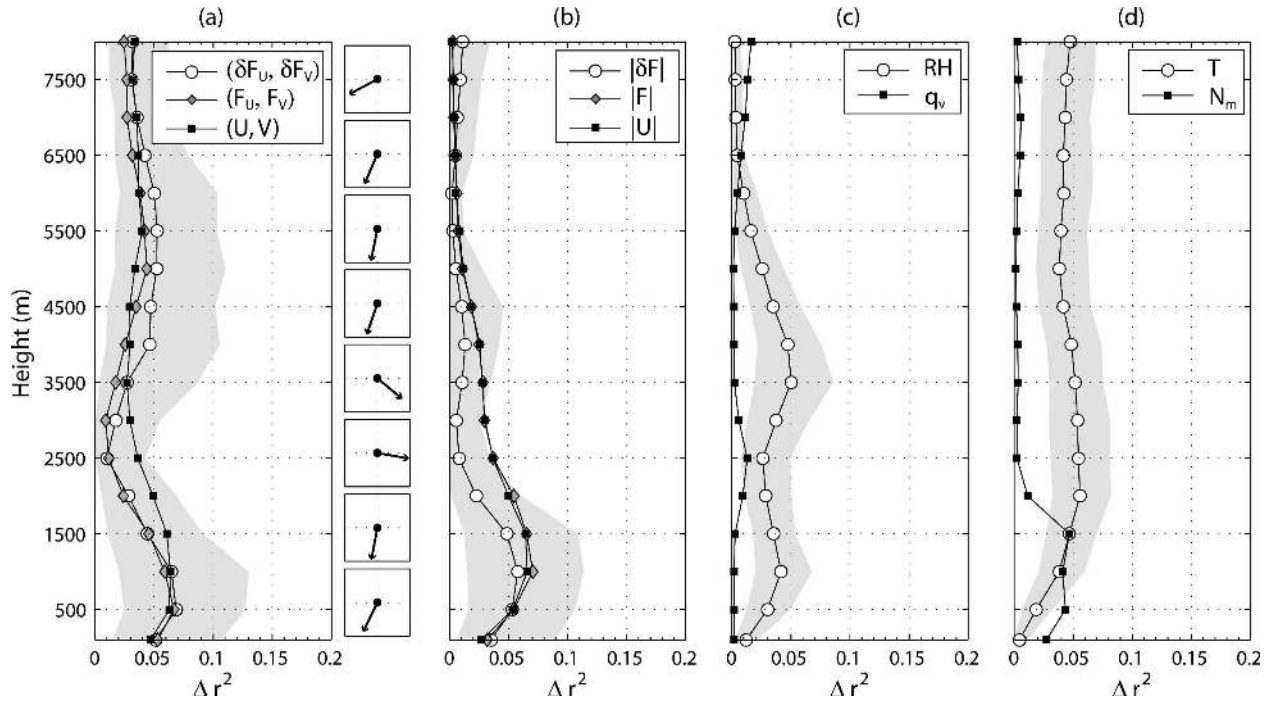
FIG. 8. Results of a multiple regression analysis in which the δF_{u2500m} is included along with all predictors tested. The goodness of fit is measured by the Δr^2 statistic, which is the increase in r^2 over that obtained using δF_{u2500m} alone. The gray shading indicates the 95% confidence regions of r^2 for predictors corresponding to the white circles. The arrows to the right of (a) indicate the direction of the component of the flux vector $(\delta F_U, \delta F_V)$ that gives the best fit to P_m.

Of all the predictors considered, the humidity-weighted moisture flux at 2500 m (δF_{u2500}) shows the strongest relation to P_m, explaining 50% of its variance. The level of maximum correlation is located slightly above the level of maximum mean zonal moisture flux during precipitation events (Fig. 6e) and is coincident with the mean freezing level (Fig. 6). It is important to emphasize that at this level it is the *zonal* component of δF that relates most strongly to P_m, despite the fact that the δF at this level is most variable in the NW–SE direction. Thus it appears that the mean precipitation in lowland central Chile responds most strongly to variation in the moisture flux oriented toward the major orographic gradients of the Andes and coastal range.

We performed a second regression analysis, similar to that described previously except that the δF_{u2500} parameter was included in all regression equations (Fig. 8). The performance of each predictor is now measured by Δr^2, defined as the increase in the r^2 statistic over the result of the regression using F_{u2500} alone. Overall, the values of Δr^2 are small ($<6\%$) for all predictors tested. Hence, once the influence of F_{u2500} on the rainfall series is taken into account, additional relationships between precipitation and the upstream conditions are relatively weak.

We have so far considered solely the area-averaged

precipitation P_m, and it is not known whether the empirical relationships are equally applicable at all locations or if they exhibit a spatial dependence. To examine this point, the regression analysis was applied to the daily precipitation records at individual stations, using all days in which the precipitation was greater than 1 mm and allowing the inclusion of days not in the combined station pool of events. Owing to the increased environmental noise in the single-station data, the correlations with upstream variables were generally smaller than those for the P_m. Nonetheless, it was found that at all sites, without exception, the pseudoflux vector δF exhibited the best relationship to the daily precipitation (in terms of r^2) of all predictors considered.

Figure 9a shows the orientation of the flux vector that gives the maximum correlation r^2 with the daily precipitation at each site. The dependence on δF is remarkably uniform despite the complex terrain of the region, being oriented in the zonal direction at the majority of sites despite the fact that the local orographic slope is oriented nonzonally at many of these locations. The strength of correlation increases north to south and at some of the southernmost stations the zonal moisture flux explains more than 60% of the daily rainfall variability. The level of maximum r^2 is generally between 1500 and 3500 m, increasing weakly from north to south
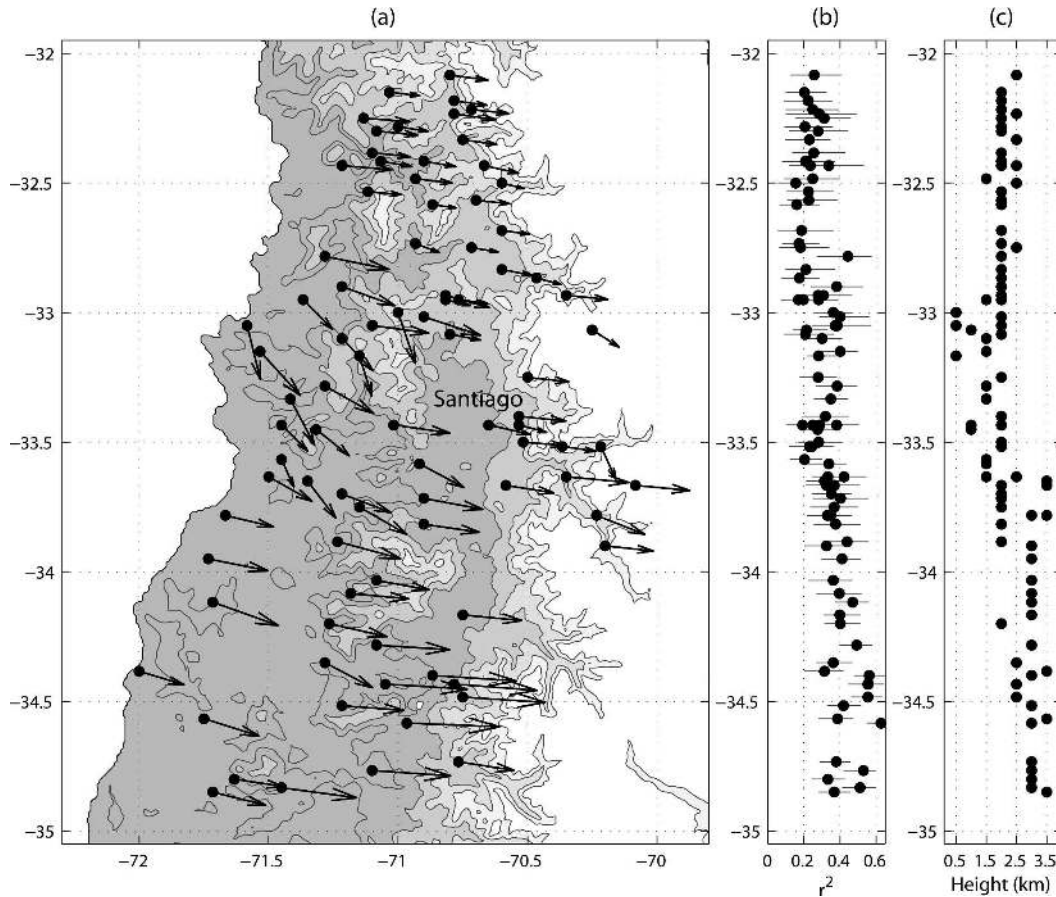
FIG. 9. (a) Results of the regression of the humidity-weighted moisture flux vector (δF_U, δF_V) against precipitation at individual rain gauges. The length of the arrows in (a) indicates r^2 at its level of maximum value, and their orientation indicates the direction of the component of the flux vector (δF_U, δF_V) that gives the best fit to the precipitation. (b) The statistic r^2 as a function of latitude and (c) the height where the r^2 is greatest.

(Fig. 9c) and with no clear dependence on topographic elevation (not shown). The southward increase in the strength of the δF_u relationship may arise because zonal moisture flux variability is likely to increase in this direction, because wind velocities along the encroaching fronts should generally increase to the south, and because mountain blocking may be reduced due to the southward decrease in the barrier height of the Andes (Fig. 2c).

6. Precipitation enhancement in the Andes

The results presented in section 4 indicate that, over long time scales, in the central part of the study domain the windward slopes of the Andes experience about two times the precipitation observed over the lowlands to the west. However, even a cursory examination of daily rainfall series reveals that this enhancement ratio is not consistently realized during individual precipita-

tion events. Instead, the degree of enhancement varies considerably, from days when the precipitation in the Andes exceeds that over the central valley by factors of 10 or more, to others when less precipitation is recorded in the Andes. In this section we explore the factors contributing to heavy orographic enhancement, or otherwise, in the Andes by contrasting the mean meteorological conditions associated with high and low enhancement events.

Time series of daily precipitation representative of the Andes and the lower terrain to the west were obtained by calculating the mean daily precipitation from two groups of three rain gauge stations situated within the upper Maipo Valley (Andes) and in the Santiago basin (see Fig. 1). The winter mean precipitations are 653 and 431 mm, respectively, giving a local climatological enhancement factor of 1.51. The data series are strictly representative of the central part of the Andes. Given the large variation in the climatological

TABLE 4. Basic rainfall statistics for the sets of precipitation events A and S and subsets defined as unif, supr, and enha; N is the number of events in each set of events; P_{Andes} and P_{Sant} are the set mean precipitation in the Andes and Santiago basin, respectively; and E is the mean precipitation enhancement, defined simply as P_{Andes}/P_{Sant}.

Group	Santiago (S)	Andes (A)	unif	supr	enha
N	75	75	35	35	35
P_{Andes}	40.1	50.7	48.6	21.9	51.2
P_{Sant}	38.2	29.7	38.7	38.2	13.7
E	1.04	1.71	1.26	0.57	3.73

enhancement ratio along the Andes (Figs. 3a,c) it is possible that the meteorological associations to orographic enhancement are different to the north and to the south.

We selected the 75 heaviest precipitation events at the Santiago basin and the Andes for further analysis. Lighter rainfall events were ignored because differences in rainfall between the lower and upper sites are more likely to be unduly influenced by stochastic precipitation variability in these cases. The pools of events for the Andes and the Santiago will be referred to A and S, respectively. As 45 events are common to both A and S the combined pool is made up of 105 events in total. Precipitation statistics are shown in Table 4 (left section). Both A and S compose about 15% of the total number rainy days over the 10 seasons but account for about 60% of the total precipitation in each location. Figure 10 plots the daily precipitation in the Santiago basin against the precipitation in the Andes. The large scatter emphasizes the fact that the heaviest rainfall events in the cordillera do not always correspond to the heaviest events in Santiago and vice versa.

The combined set precipitation events (S ∪ A) were divided into three groups, each with 35 members, based on the amount of orographic enhancement (E), defined as the ratio of precipitation in the Andes to that in the Santiago basin. The upper tercile we define as consisting of enhancement (enha) events; the mean enhancement factor being nearly 4 (3.73) for these events (Table 4). The middle and lower terciles are labeled as uniform (unif) and suppressed (supr), respectively; these names reflect the fact that E is near-unity (1.26) for the unif events and significantly less than unity for
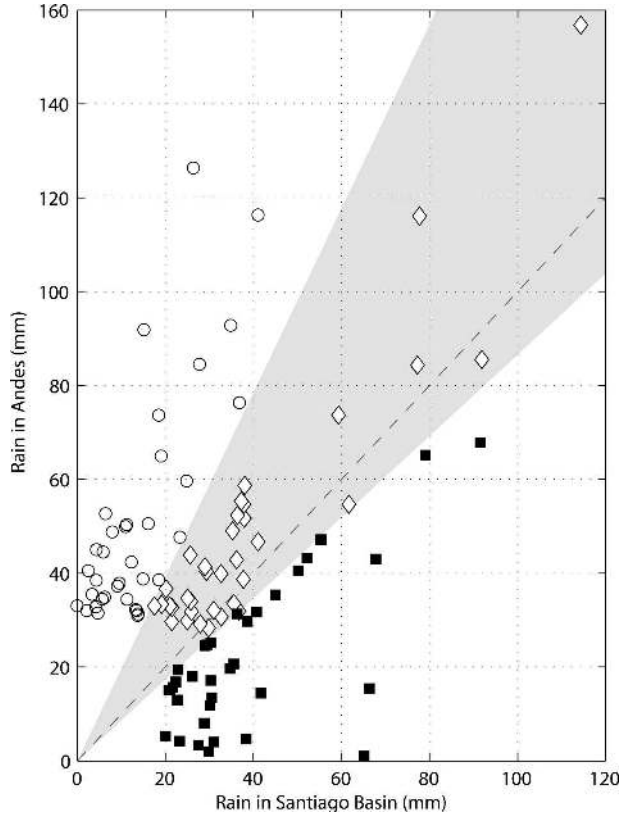

FIG. 10. Scatterplot of precipitation for the 75 strongest daily rainfall episodes in Santiago (group S) and in the Andes (group A), which add up to 105 events in total. Circles, diamonds, and squares indicate events classified as enha, unif, and supr, respectively. The gray area is that between the rainfall enhancement ratio (E) limits used to define the three event categories. The dashed line indicates a 1:1 rainfall ratio.

the supr events (Table 4). This classification methodology is similar to that used by Dettinger et al. (2004) in their study of precipitation enhancement in the Sierra Nevada range.

Figures 11a–c show the mean spatial patterns of precipitation across the entire rain gauge network for each of the three enhancement categories. Both the supr and unif groups have a homogeneous pattern over the coastal zone and central valley, with only slight meridional increase (Figs. 11b,e), and precipitation recorded in close to 100% of events at stations south of 33°S (Fig. 11c,f). The precipitation frequency drops farther to the

→

FIG. 11. Mean daily precipitation (P_d) and precipitation frequency (P_f) for the (top) supr, (middle) unif, and (bottom) enhc groups. The maps show the P_d at each station, while the central and rightmost panels show the P_d and P_f against station latitude. The P_f at a given station is defined as the percentage of days in which precipitation was recorded. The white square shows the location of Santiago.
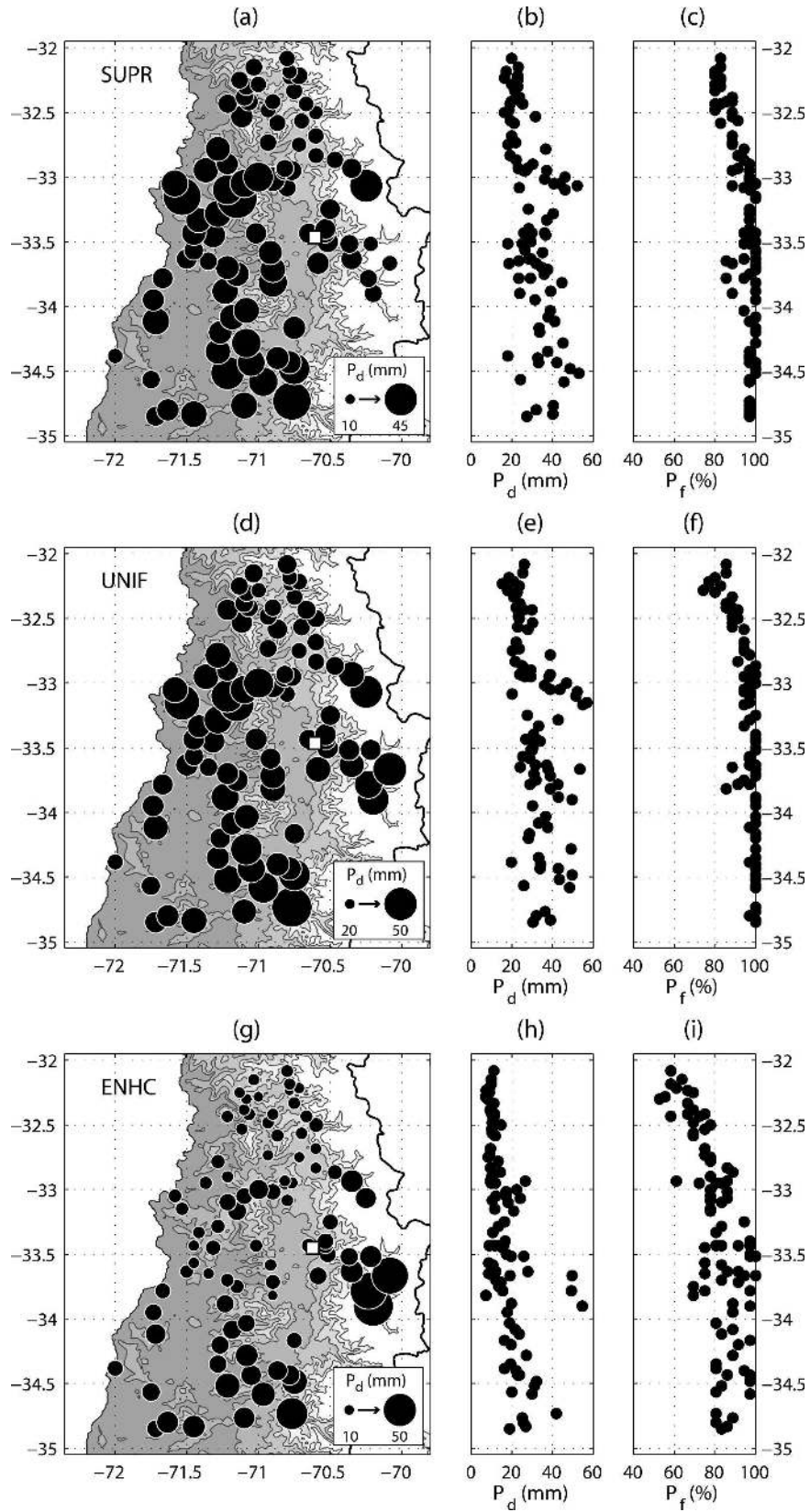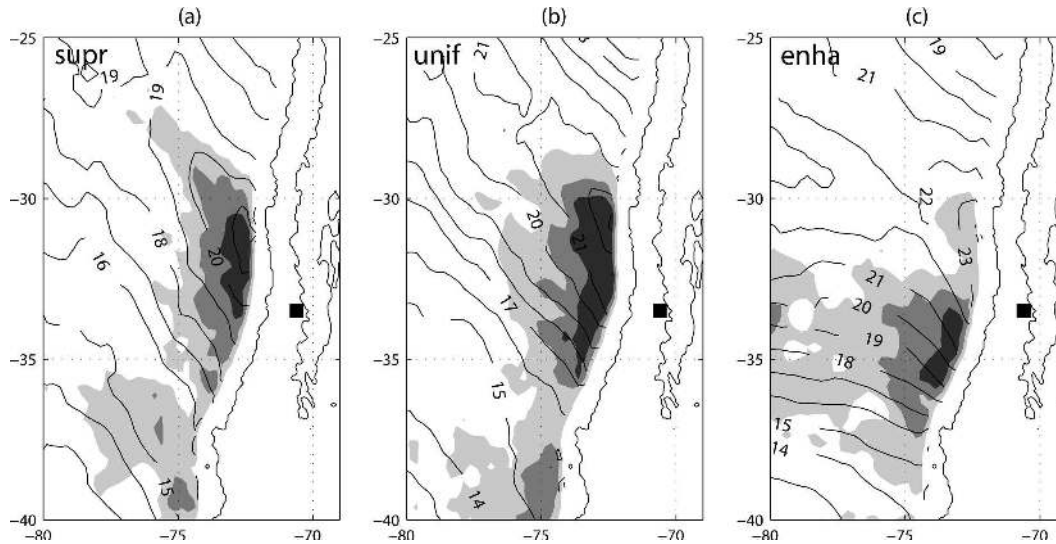
FIG. 12. Composites of SSM/I total precipitable water (solid lines) and precipitation frequency P_f (shaded contours) for the (a) supr, (b) unif, and (c) enha groups. Light, medium, and dark gray shading represent the P_f ranges 20%–30%, 30%–40%, and >40%, respectively. Units of precipitable water are mm. The black square indicates the location of Santiago.

north but remains above 80% at most stations. Consistent with its definition, the enha group shows a local precipitation maximum in the Andes west of Santiago (Fig. 11g). Over the rest of the domain the precipitation pattern is characterized by a marked south to north decrease in the mean daily precipitation. South of Santiago (33.4°S), precipitation was recorded on over 80% of days at most sites (Fig. 11i), but farther north the frequency of precipitation drops sharply, indicating that during enha events rainfall is generally concentrated in the southern half of central Chile.

Figures 12a–c show composites of SSMI/I rainfall frequency and precipitable water over the ocean to the west of central Chile for the three categories supr, unif, and enha, which visual inspection confirms are representative of the situations found in individual cases. All three composites show the characteristic cold frontal pattern discussed in section 4: a long tongue of moist air impinging on central Chile with a rainfall zone on its southern side. They differ mainly in the meridional displacement of this pattern. In the unif and supr composites, the oceanic precipitation is positioned to the north of Santiago. Inspection of individual cases reveals that frontal rainbands are usually aligned steeply with respect to the axis of the cordillera and, extrapolating visually, cross directly over central Chile consistent with the widespread precipitation observed in these cases. During enha events the oceanic precipitation is concentrated to the south of Santiago, again consistent with the terrestrial precipitation pattern. The synoptic precipitation in these events is typically organized into

zonal rainbands, with central Chile placed squarely in the prefrontal sector.

In keeping with their prefrontal character, the enha events are associated with warmer, more stable conditions at the coastal radiosonde site (Fig. 13). The 700-m difference in freezing-level height between enha and supr/unif categories amounts to a column mean temperature difference of about 5 K. From the profiles of relative humidity (Fig. 13b) it is seen that the unif events have the highest humidities throughout most of the column. The enha group is the driest at lower altitudes (<3700 m), while the supr group is driest at higher altitudes. The N_w^2 profiles (Fig. 13c) show mean conditional instability below 2000 m in the unif and supr groups, while stable conditions prevail in this layer for enha events.

The shapes of the mean profiles of zonal moisture flux (Fig. 13a) for supr and unif events are similar to the climatological mean (Fig. 6e). Both have maximum values near 2200 m, the mean F_u at this level being greatest for the unif events, in keeping with the higher mean rainfall for this group (cf. the results of the previous section). The enha F_u profile is characterized by a broader peak and significantly higher F_u at mid- to upper levels (i.e., >4000 m). At the altitude of 5000 m (the approximate height of the Andes Cordillera) the F_u is nearly twice that of the unif and supr composites. The stronger midlevel moisture fluxes in the enha composites are due in roughly equal parts to higher zonal wind speeds and higher water vapor mixing ratios (not shown).
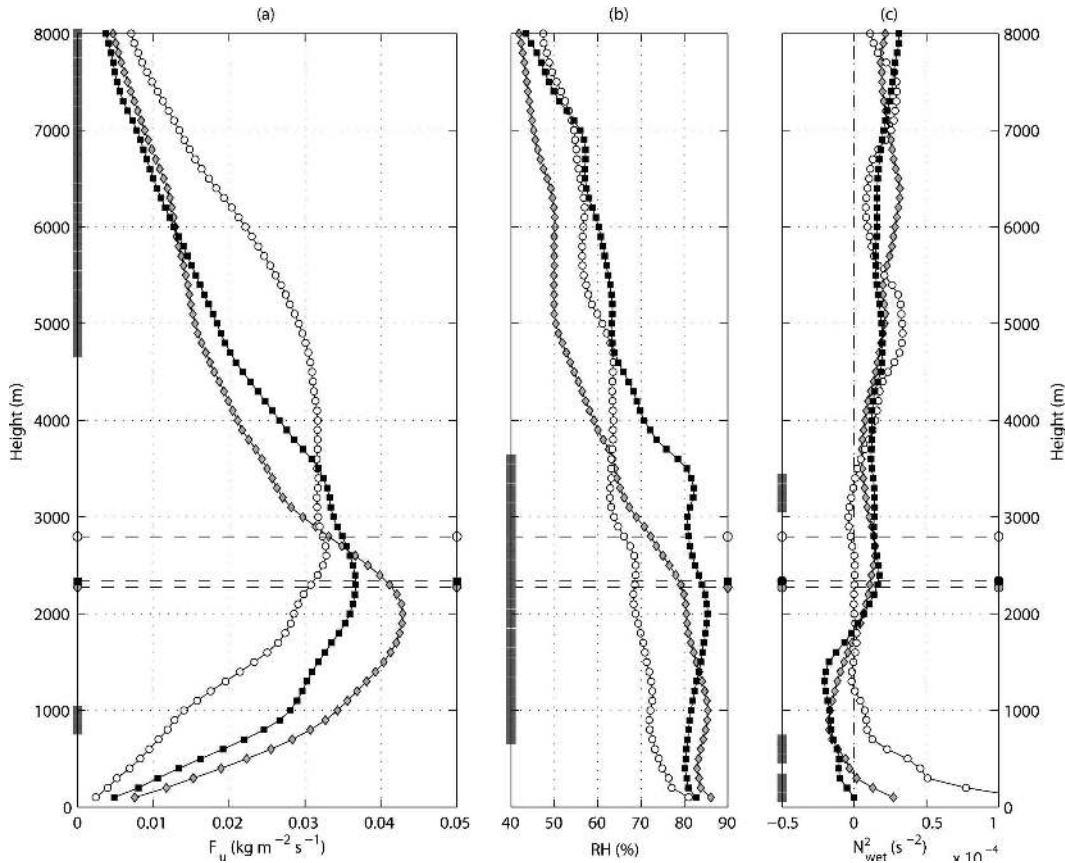
FIG. 13. Mean radiosonde profiles of (a) $\mathbf{F}_u$, (b) RH, and (c) N_{wet} for precipitation episodes classified as enha (white circles), unif (gray diamonds), and supr (black squares). The dashed horizontal lines in all panels indicate the mean freezing levels for each group. Gray bars on the left-hand side of each panel indicate those levels where the difference in the mean between the enha and supr groups is significant at the 95% confidence level.

The results of this section imply that precipitation enhancement in the Andes is closely tied to the phase of frontal passage. Heavy precipitation in Santiago (both the supr and unif events) is associated with cases of widespread precipitation produced as frontal rainbands cross central Chile. Although the precipitation in the Andes is highly variable in these cases, the mean precipitation enhancement is negligible ($E = 1.04$; Table 4). Events of high precipitation enhancement (enha) in the Andes tend to occur in the warmer prefrontal sector on occasions where the midlevel moisture flux is sufficient to initiate heavy precipitation in the cordillera. Our results are paralleled by those of Dettinger et al. (2004) who performed a similar study in California's central Sierra Nevada, a mountain range whose geometry, altitude, and climatic setting are similar to the Andes of central Chile. They also found that high and low orographic enhancement events also occurred in distinct sectors of the associated baroclinic systems. However, they obtained the opposite relationship, with the highest (weakest) orographic enhancement occurring in the cold (warm) sectors.

The (humidity weighted) moisture flux at 2500 m was found in the previous section to be strongly related to the precipitation intensity throughout the study area. It is therefore interesting to note that the mean F_{u2500} is similar for the enha and supr groups despite the fact that the mean precipitation recorded at most low-lying stations is weaker during enha cases, indicating that the zonal moisture flux at lower levels does not generate much precipitation in low-lying regions during the prefontal situations that characterize the enha group. It seems likely that the presence of synoptic-scale precipitation may be a critical ingredient for the production (e.g., via "seeder feeder" processes; Carruthers and Choularton 1983) of heavy rainfall in the low-level flows associated with F_{u2500} and may in itself constitute a substantial component of the total precipitation that reaches the surface. Moreover, the higher stability and lower relative humidity of the low-

level flow (Fig. 13c) may prevent the initiation of precipitation at low altitudes in the *enha* cases.

7. Discussion

A perhaps surprising aspect of the precipitation in central Chile is the apparent uniformity of the precipitation distribution in the cross-mountain direction, particularly evident in the frontal (unif and supr) cases examined in the previous section. There may be several explanations for this. First, the rain gauge network does not adequately sample precipitation in the parts of the study area where topographic gradients are strongest, and the existence of coherent zones of long-term precipitation enhancement is not precluded by the observational data we have examined. Second, the weak cross-mountain winds, which rarely exceed 10 m s^{-1} below 2000 m, will severely limit the magnitude of topographically forced updrafts, especially over lower-elevation coastal features. Third, the synoptic-scale precipitation produced aloft in the frontal rainbands, which will be less affected by the orography, may often dominate the surface precipitation pattern.

Nonetheless, the statistical analysis of section 5, which made no advance assumptions regarding the optimal height or direction of the flux vector, found an optimal relationship between precipitation and the *zonal* component of moisture flux (multiplied by relative humidity) at a height near to its climatological peak consistent with the idea that orographic ascent embedded within the fronts that cross central Chile is to some degree modulating precipitation intensities. The dependence on δF_u is significant at all stations, not just those situated on strongly sloping topography. Hence, insofar as the F_u relationship represents an orographic forcing, the concomitant orographic processes must act to distribute the precipitation relatively evenly between the coast and the Andes.

A number of observational and theoretical results have shown that under stable conditions orographic lifting may extend upstream of the upwind slopes of the responsible orographic features. Neiman et al. (2002) examined several cases in California's coastal mountains when low-level upslope flow was blocked, finding that in these situations topographic modulation of the rainfall pattern was weak, but precipitation rates were nonetheless strongly correlated with cross-mountain winds. They proposed that isentropic lifting over an upstream layer of stagnant, blocked air resulted in orographic uplift extending well upwind of the coastal orography (see their Fig. 19). This conclusion is supported by radar observations of the upstream flow structure during frontal rainstorms that have been pre-

sented for the European Alps (Bousquet and Smull 2003; Medina and Houze 2003) and Washington's Cascades (Medina et al. 2005). These studies indicate that a stably stratified layer of weak or reversed cross-mountain flow, sloping smoothly upstream toward the mountain crest, is a persistent feature of the cross-mountain flow structure ahead of large mountain ranges under blocked conditions (Medina et al. 2005). In these cases the production of small-scale updraft cells by turbulence in the shear layer between the stagnant layer and free atmosphere above was found to play an important role in the precipitation process (Houze and Medina 2005).

Other mechanisms, such as the upstream tilting of gravity waves in low Froude number flows (Smith 1979; Wratt et al. 2000) and the upstream triggering (followed by downstream advection) of convective circulations (Chu and Lin 2000) may also diffuse the orographic precipitation pattern in low Froude number situations, yet retain a strong dependence on the strength of cross-mountain flow.

We caution that the interpretation of the empirical δF_u relationship as being representative of a purely orographic interaction may be misleading, since the strength of synoptic-scale precipitation may also be statistically related to moisture flux (Rasmussen et al. 2001). This possibility is partially demonstrated in the last column of Table 2, which shows that the zonal moisture flux also increases with the frontal precipitation index (I_{front}) defined in section 4. Furthermore, the results of the previous section indicate that the frontal and orographic precipitations are not only linked statistically but physically since some environmental preconditioning, such as conditional instability or seeder precipitation, appears necessary for moist low-level flows to generate rainfall. The recent studies of Medina and Houze (2003) and Houze and Medina (2005) have provided detailed examples of the character of rainfall production within frontal systems in the European Alps and Washington's Cascades, which reveal the precipitation falling in the baroclinic system to be a key player in the orographic enhancement process. In addition, the frontal circulations themselves may be strongly modified by orography (e.g., Egger and Hoinka 1992). For example, in a numerical case study of a front crossing central Chile, Falvey and Garreaud (2005) found that the formation of a northerly barrier flow in the warm sector could enhance low-level convergence, and hence precipitation, along the frontal boundary [Neiman et al. (2004) observed a similar event upstream of California's coastal range]. It is possible that this indirect enhancement mechanism, should it be a recurring phenomena, may be statistically related to the strength of

cross-mountain flow (which determines barrier jet formation) and thus influences the δF_u dependencies found in section 5.

8. Conclusions

In this study wintertime precipitation in central Chile was examined using daily observations from precipitation gauge, radiosonde, and SSM/I passive microwave radiometer over a 10-winter period from 1993 to 2002.

Wintertime precipitation episodes typically occur as cold fronts pass over the region from west to east, and the synoptic-scale precipitation may constitute a major component of the precipitation observed over land areas. On rainy days, a cross-mountain component of flow prevails throughout the lower troposphere, but there is weakening and northerly deviation of the flow at lower levels, symptomatic of both large-scale wind shear in the baroclinic system and blocking due to the Andes. The long-term precipitation pattern is dominated by a climatological north–south gradient, mainly due to a northward decrease in the frequency of precipitation events. The influence of the Andes extends several hundred kilometers upstream. Over the mainland, winter precipitation is quite uniform between the coast and the base of the Andes, despite a complex coastal topography. Long-term enhancement is observed on the western slopes of the Andes, where enhancement factors of between one and three, increasing north to south, are observed. The precipitation enhancement in the Andes may vary greatly from one event to the next. Heavy, but isolated, precipitation in the Andes tends to occur in the warmer, prefrontal sector of approaching storms and is associated with unusually high moisture fluxes near to and above the crest of the mountain range. Strongly frontal episodes, characterized by widespread rainfall throughout central Chile, lead to variable, but on average rather weak, enhancement in the Andes. Our conclusions regarding the spatial pattern of precipitation are limited by a poor sampling of high-altitude rain gauges, both in the coastal range and in the Andes.

Regression analysis against coastal radiosonde observations indicates that daily precipitation is most strongly related to the humidity-weighted moisture flux in the zonal direction at an altitude near to that of the maximum mean zonal flux during precipitation events (2500 m). The relationship to zonal moisture flux is significant at all stations. The dependence of precipitation on the zonal moisture flux is suggestive of an interaction with the major orographic gradients of the Andes and coastal range, although it is recognized that frontal precipitation may exhibit similar dependencies.

The results of this study have provided information on the general associations between the upstream conditions, topography, and precipitation in central Chile and allow us to make some initial suggestions regarding the orographic interactions likely to be especially important in the region. However, the establishment of firm links between the statistical relationships found in this study and corresponding physical processes will require closer examination of individual events. Detailed observational studies, possibly complemented by numerical simulation, are therefore the natural next step toward a more comprehensive understanding of the influence of central Chile's imposing topography on regional precipitation patterns.

APPENDIX

Calculation of Wintertime Precipitation from River Discharge Measurements

Here we discuss in more detail the methodology used to make the estimates of winter rainfall from river discharge measurements in the Andes (Table 1). The watersheds are all very high altitude, most of them lining the western rim of the Andes with mean altitudes in excess of 3000 m. River discharges are predominantly from snowmelt, exhibiting a characteristic annual discharge cycle of opposite phase to the annual precipitation cycle.

Following Sankarasubramanian and Vogel (2002), the annual water balance in a given watershed may be expressed as

$$dS/dt = AR^* - Q - E - G. \qquad (A1)$$

In this equation (actually valid over all time scales) the net annual change in water storage dS/dt (m^3 yr^{-1}) is equal to the mean annual precipitation, R^* (m yr^{-1}), in the water shed of area A (m^2) minus losses from river discharge at the catchment outlet point (Q), evaporation + sublimation (E), and groundwater runoff (G).

Estimation of R^* from Q alone, without recourse to complex distributed surface models, relies on the assumption that the E, G, and dS/dt terms are either small

compared to Q and AR^* or that they can be accurately estimated. Setting these terms to zero allows a rough estimate of a minimum value for basin precipitation assuming that all precipitation exits the watershed via river discharge. Neglecting the possibility of fissures, the hard rock aquifers of the Andes are relatively impermeable with negligible vegetation cover, and the time period from which the mean annual discharge values are derived (30 yr) is very long; thus, these assumptions are not entirely unreasonable.

The evaporation term (E) forms a substantial part of the water balance in most watersheds. The watersheds considered in this study are mostly covered by the snowpack that forms after the first few storms of each year, and E is principally due to sublimation, a process exacerbated by the extremely dry atmosphere above the central Andes in nonrainy circumstances (RH < 40%). There are few observations of sublimation rates in the Andes of central Chile, which makes estimation of even a rough value for E somewhat difficult. Based on field observations and modeling on the Juncal Norte and Lomo Larga glaciers, both of which are within our study domain, Corripio and Purves (2005) concluded that sublimation rates may exceed 6 mm day^{-1} and average 2 mm day^{-1} during the ablation season. We also examined the surface moisture fluxes produced from an extended Weather Research and Forecasting (WRF) mesoscale model simulation for the winter of 2002. The model, which made use of the six-layer Rapid Update Cycle surface model (Benjamin et al. 1998), gave average surface moisture fluxes of 0.8 mm day^{-1} over snow-covered surfaces in the central Andes. Taking the mean of the above estimates, we conclude that over the 6–8-month period from the formation of the winter snowpack until its disappearance at the end of the ablation season, sublimation rates may (very roughly) average around 1.5 mm day^{-1}.

Other terms in Eq. (A1) are expected to be relatively small. Some of the watersheds are partially glaciated (Casassa 1995), and over the 30-yr period of the streamflow observations, glacial melt is expected to make a small negative contribution to the dS/dt term (Rivera et al. 2002; Carrasco et al. 2005), although glacial growth (with a corresponding positive impact on dS/dt) may also have occurred on individual years (Fountain and Tangborn 1985). The G term is expected to be very small in relation to the streamflow term Q, since, in comparison with stream velocities, the movement of groundwater, even in the best groundwater reservoirs, is extremely slow [American Society of Civil Engineers (ASCE) 1996]. In any case, even a crude estimation of G requires detailed geological information, particularly near the river discharge site, which was not available for this study.

Based on the preceding discussion, we use the following simple formulas to estimate lower and upper limits, R^*_{w1} and R^*_{w2}, for the catchment mean *wintertime* precipitation:

$$R^*_{w1} = 0.90\,Q/A \quad \text{and} \tag{A2}$$

$$A_{snow}/AR^*_{w2} = 0.90\,Q/A + 300\,A_{snow}/A, \tag{A3}$$

where both R^*_{w1} and R^*_{w2} are in millimeters, and A_{snow} is the area of the watershed above the snow line. The factor of 0.90 before the first term of Eqs. (A2) and (A3) takes into account the fact that about 90% of the total rainfall in the Andes occurs during winter. The second term in Eq. (A3) assumes a mean sublimation rate of 1.5 mm day^{-1} over a 200-day period, which represents the typical duration of the winter snowpack. Implicit in this equation is the assumption that the average snowfall in the watersheds is at least 300 mm. From the data presented in section 4, this assumption seems reasonable, except perhaps in the northernmost watersheds.

REFERENCES

Aceituno, P., 1988: On the functioning of the Southern Oscillation in the South American sector. Part I: Surface climate. *Mon. Wea. Rev.,* **116,** 505–524.

American Society of Civil Engineers (ASCE), 1996: *Hydrology Handbook*. 2d ed. ASCE, 800 pp.

Banta, R. M., 1990: The role of mountain flows in making clouds. At*mospheric Processes over Complex Terrain, Meteor. Monogr.,* No. 45, Amer. Meteor. Soc., 229–283.

Bell, T. L., and P. N. Kundu, 2000: Dependence of satellite sampling error on monthly averaged rain rates: Comparison of simple models and recent studies. *J. Climate,* **13,** 449–462.

Benjamin, S. G., J. M. Brown, K. J. Brundage, B. E. Schwartz, T. G. Smirnova, and T. L. Smith, 1998: RUC-2—The Rapid Update Cycle version 2. NWS Tech. Procedures Bulletin 448, NOAA/NWS, 18 pp.

Berg, W., and S. K. Avery, 1995: Evaluation of monthly rainfall estimates derived from the Special Sensor Microwave/Imager (SSM/I) over the tropical Pacific. *J. Geophys. Res.,* **100** (D1), 1295–1316.

Bousquet, O., and B. F. Smull, 2003: Observations and impacts of upstream blocking during a widespread orographic precipitation event. *Quart. J. Roy. Meteor. Soc.,* **129,** 391–409.

Carlson, T. N., 1998: *Mid-Latitude Weather Systems*. Amer. Meteor. Soc., 507 pp.

Carrasco, J. F., G. Casassa, and J. Quintana, 2005: Changes of the 0°C isotherm and the equilibrium line altitude in central Chile during the last quarter of the 20th century. *Hydrol. Sci. J.,* **50,** 933–948.

Carruthers, D. J., and W. T. Choularton, 1983: A model of the feeder-seeder mechanism of orographic rain including stratification and wind-drift effects. *Quart. J. Roy. Meteor. Soc.,* **109,** 575–588.

Casassa, G., 1995: Glacier inventory in Chile: Current status and recent glacier variations. *Ann. Glaciol.,* **21,** 317–322.

Chu, C.-M., and Y.-L. Lin, 2000: Effects of orography on the generation and propagation of mesoscale convective systems in a two-dimensional conditionally unstable flow. *J. Atmos. Sci.,* **57,** 3817–3837.

Corripio, J. G., and R. S. Purves, 2005: Surface energy balance of high altitude glaciers in the central Andes: The effect of snow penitentes. *Climate and Hydrology in Mountain Areas,* C. de Jong, D. Collins, and R. Ranzi, Eds., Wiley & Sons, 15–29.

Dettinger, M., K. Redmond, and D. Cayan, 2004: Winter orographic precipitation ratios in the Sierra Nevada—Large-scale atmospheric circulations and hydrologic consequences. *J. Hydrometeor.,* **5,** 1102–1106.

Durran, D. R., and J. B. Klemp, 1982: The effects of moisture on the Brunt–Väisälä frequency. *J. Atmos. Sci.,* **39,** 2152–2158.

Efron, B., and R. J. Tibshirani, 1993: *An Introduction to the Bootstrap.* Chapman and Hall, 436 pp.

Egger, J., and K. P. Hoinka, 1992: Fronts and orography. *Meteor. Atmos. Phys.,* **48,** 3–36.

Falvey, M., and R. D. Garreaud, 2005: A numerical case study of an orographically enhanced frontal system in central Chile. *Croat. Meteor. J.,* **40,** 486–489.

Fountain, A. G., and W. V. Tangborn, 1985: The effect of glaciers on streamflow variations. *Water Resour. Res.,* **21,** 579–586.

Fuenzalida, H., R. Sanchez, and R. Garreaud, 2005: A climatology of cut off lows in the Southern Hemisphere. *J. Geophys. Res.,* **110,** D1801, doi:10.1029/2005JD005934.

Garreaud, R., and Y. J. Rutllant, 1996: Análisis meteorológico del los aluviones de Antofagasta y Santiago de Chile en el periodo 1991–1993. *Atmósfera,* **9,** 251–271.

Grimm, A., V. Barros, and M. Doyle, 2000: Climate variability in southern South America associated with El Niño and La Niña events. *J. Climate,* **13,** 35–58.

Hayes, P., L. A. Rasmussen, and H. Conway, 2002: Estimating precipitation in the central Cascades of Washington. *J. Hydrometeor.,* **3,** 335–346.

Hill, F. F., K. A. Browning, and M. J. Bader, 1981: Radar and rain gauge observations of orographic rain over south Wales. *Quart. J. Roy. Meteor. Soc.,* **107,** 643–670.

Houze, R. A., 1993: *Cloud Dynamics.* International Geophysics Series, Vol. 53, Academic Press, 573 pp.

——, and S. Medina, 2005: Turbulence as a mechanism for orographic precipitation enhancement. *J. Atmos. Sci.,* **62,** 3599–3623.

Kalnay, E., and Coauthors, 1996: The NCEP/NCAR 40-Year Reanalysis Project. *Bull. Amer. Meteor. Soc.,* **77,** 437–471.

Medina, S., and R. A. Houze Jr., 2003: Air motions and precipitation growth in alpine storms. *Quart. J. Roy. Meteor. Soc.,* **129,** 345–371.

——, B. F. Smull, R. A. Houze Jr., and M. Steiner, 2005: Cross-barrier flow during orographic precipitation events: Results from MAP and IMPROVE. *J. Atmos. Sci.,* **62,** 3580–3598.

Montecinos, A., and P. Aceituno, 2003: Seasonality of the ENSO-related rainfall variability in central Chile and associated circulation anomalies. *J. Climate,* **16,** 281–296.

——, A. Diaz, and P. Aceituno, 2000: Seasonal diagnostic and predictability of rainfall in subtropical South America based on tropical Pacific SST. *J. Climate,* **13,** 746–758.

Neiman, P. J., F. M. Ralph, A. B. White, D. E. Kingsmill, and P. O. G. Persson, 2002: The statistical relationship between upslope flow and rainfall in California's coastal mountains—Observations during CALJET. *Mon. Wea. Rev.,* **130,** 1468–1492.

——, P. O. G. Persson, F. M. Ralph, D. P. Jorgensen, A. B. White, and D. E. Kingsmill, 2004: Modification of fronts and precipitation by coastal blocking during an intense landfalling winter storm in southern California: Observations during CALJET. *Mon. Wea. Rev.,* **132,** 242–273.

Overland, J. E., and N. A. Bond, 1993: The influence of coastal orography: The Yakutat storm. *Mon. Wea. Rev.,* **121,** 1388–1397.

——, and ——, 1995: Observations and scale analysis of coastal wind jets. *Mon. Wea. Rev.,* **123,** 2934–2941.

Pandey, G. R., D. R. Cayan, and K. P. Georgakakos, 1999: Precipitation structure in the Sierra Nevada of California during winter. *J. Geophys. Res.,* **104** (D10), 12 019–12 030.

——, ——, M. D. Dettinger, and K. P. Georgakakos, 2000: A hybrid model for interpolating daily precipitation in the Sierra Nevada of California during winter. *J. Hydrometeor.,* **1,** 491–506.

Pizarro, J. G., and A. Montecinos, 2000: Cutoff cyclones off the subtropical coast of Chile. Preprints, *Sixth Int. Conf. on Southern Hemisphere Meteorology and Oceanography,* Santiago, Chile, Amer. Meteor. Soc., 278–279.

Rasmussen, L. A., and W. V. Tangborn, 1976: Hydrology of the North Cascades region, Washington. 1: Runoff, precipitation, and storage characteristics. *Water Resour. Res.,* **12,** 187–202.

——, H. Conway, and P. S. Hayes, 2001: Estimating Olympic Peninsula precipitation from upper air wind and humidity. *J. Geophys. Res.,* **106,** 1493–1501.

Rivera, A., C. Acuña, A. G. Casassa, and F. Bown, 2002: Use of remotely sensed and field data to estimate the contribution of Chilean glaciers to eustatic sea-level rise. *Ann. Glaciol.,* **34,** 367–372.

Roe, G. H., 2005: Orographic precipitation. *Annu. Rev. Earth Planet. Sci.,* **33,** 645–671.

Rutllant, J., and H. Fuenzalida, 1991: Synoptic aspects of the central Chile rainfall variability associated with the Southern Oscillation. *Int. J. Climatol.,* **11,** 63–76.

Saavedra, N., and A. J. Foppiano, 1992: Monthly mean pressure model for central Chile. *Int. J. Climatol.,* **12,** 469–480.

Sankarasubramanian, A., and R. M. Vogel, 2002: Annual hydroclimatology of the United States. *Water Resour. Res.,* **38,** 1083–1093.

Sinclair, M. R., 1994: A diagnostic model for estimating orographic precipitation. *J. Appl. Meteor.,* **33,** 1163–1175.

Smith, E. A., and Coauthors, 1998: Results of WetNet PIP-2 Project. *J. Atmos. Sci.,* **55,** 1483–1536.

Smith, R. B., 1979: The influence of mountains on the atmosphere. *Advances in Geophysics,* Vol. 21, Academic Press, 87–230.

Smolarkiewicz, P. K., and R. Rotunno, 1990: Low Froude number flow past three-dimensional obstacles. Part II: Upwind flow reversal zone. *J. Atmos. Sci.,* **47,** 1498–1511.

Wentz, F. J., 1997: A well-calibrated ocean algorithm for SSM/I. *J. Geophys. Res.,* **102,** 8703–8718.

Wilks, D. S., 1995: *Statistical Methods in the Atmospheric Sciences: An Introduction.* Academic Press, 467 pp.

Wratt, D. S., M. J. Revell, M. R. Sinclair, W. R. Gray, R. D. Henderson, and A. M. Chater, 2000: Relationships between air mass properties and mesoscale rainfall in New Zealand's Southern Alps. *Atmos. Res.,* **52,** 261–282.